A 300-YEAR RECORD OF EXTREME FLOODS ON THE FRENCH BROAD RIVER, TENNESSEE

by

ALEXANDER CHASE QUIMBY

LISA DAVIS, COMMITTEE CHAIR
MATTHEW THERRELL
TESSA HARDEN

A THESIS

Submitted in partial fulfillment of the requirements
for the degree of Master of Science
in the Department of Geography
in the Graduate School of
The University of Alabama

TUSCALOOSA, ALABAMA

2023

ABSTRACT

Streamflow records in the southeastern United States are comparatively short (<100 years), resulting in higher uncertainties associated with estimates of extreme flood frequencies. Extreme floods, for the purposes of this thesis, include floods having an annual exceedance probability of 0.01 or smaller (i.e., a recurrence interval greater than or equal to 100 years). Uncertainty of flood frequency models can be reduced by including paleoflood hydrologic data, in which flood data are reconstructed from analyses of sediment deposits or tree-ring records. In this thesis, a paleoflood chronology was developed for the French Broad River, a major tributary of the Tennessee River, based on sampling and analyses conducted at an upstream floodplain (DT3A) site and a downstream rock shelter (DRS) site. A sediment core taken from DT3A was analyzed using laser granulometry to determine particle size of each centimeter of the core. Large flood events were identified based on the volume of sand and statistical analyses were used to eliminate sedimentological changes stemming from factors other than floods, using end member modeling and change point analysis. LOESS regression modeling was used to identify discrete, large magnitude paleofloods based on peaks (positive residuals) in sand volume. Paleoflood discharges were estimated using step-backwater modeling in HEC-RAS based on paleostage indicators found at DRS. Stratigraphic descriptions and floods ages (determined with radiocarbon dating) were used to identify three paleoflood events preserved at two different topographic levels at DRS. The paleoflood discharges and age information were combined with the modern gauge record and a new flood record for the French Broad River was developed that

extends an additional 250+ years. Comparing the reconstructed chronology of flood events, to similar records in the southeastern United States, it appears that extreme flood events coincide with climate transitions.

LIST OF ABBREVIATIONS AND SYMBOLS

IPCC	Intergovernmental Panel on Climate Change
USGS	United State Geological Survey
PFHA	Probabilistic Flood Hazard Assessment
PSI	Paleostage Indicator
ENSO	El Niño-Southern Oscillation
PDO	Pacific Multidecadal Oscillation
AMO	Atlantic Multidecadal Oscillation
LIA	Little Ice Age
MCA	Medieval Climate Anomaly
SWD	Slackwater Deposit
FFA	Flood Frequency Analysis
AEP	Annual Exceedance Probability
TN	Tennessee
TVA	Tennessee Valley Authority
DRS	Douglas Rock Shelter
DT	Douglas Tailwater
PSA	Particle Size Analysis
OSL	Optically Stimulated Luminescence
EMMA	End-Member Modeling

CPA	Change Point Analysis
LOESS	Locally Weighted Smoothing
ADM	Age Depth Model
HEC-RAS	Hydrologic Engineering Center's River Analysis System
RS	River Station
DEM	Digital Elevation Model
n	Manning's n
Q	Discharge
K	conveyance
A	Flow Area
R	Hydraulic Radius
S_f	Frictional Slope
PDSI	Palmer Drought Severity Index

ACKNOWLEDGEMENTS

I would like to express my deepest gratitude to my graduate research advisor, Dr. Lisa Davis for giving me an amazing opportunity to conduct research in the Fluvial Geomorphology Group. Thank you for taking a chance on a chemistry student and bringing me into the amazing world of paleoflood hydrology. This research also would not be possible without the guidance and input from the committee members Dr. Matthew Therrell and Dr. Tessa Harden. Additionally, this project would not have been possible without funding provided by the Tennessee Valley Authority. I would also Like to thank Miles Yaw and Curt Jawdy from the TVA for providing crucial feedback as well as invaluable data without which this project could not be completed. Words cannot express my gratitude to Matt Gage for his assistance in field work, obtaining the proper permits and landowner consent, and providing transportation for this research project.

I would like to extend a sincere thanks to lab mates Dr. Ray Lombardi, Dan West, and Joni Corbin for the conversations that we had throughout this project. An Additional thanks to Dr. Ray Lombardi for assisting with field work required for this research. I would also like to thank the undergraduates of the Fluvial Geomorphology Group for assisting with lab work and sample collection. Thanks, should also go to my fellow graduate students from the geography, geology, chemistry, and engineering department for conversations about this research.

Lastly, I would like to mention my family, friends, and mentors. This research would not have been possible without their belief in me and their endless support and motivation.

CONTENTS

LIST OF TABLES

LIST OF FIGURES

1. INTRODUCTION

1.1 Introduction

On average each flood event that occurs around the world claims the life of one person (Jonkman, 2005). From 1932 to 1997 the United States saw an increase in the total flood damage of 2.92% per year (Pielke and Downton, 2000). This trend is likely to continue, if not increase, over the next several decades due to an expected increase in the frequency of floods from anthropogenic changes (Milly et al., 2002), including urbanization, carbon emissions, deforestation, and climate change (Chang et al., 2008; Li-An et al., 2018). The National Weather Service predicts that in 2022 approximately 80 million Americans will be at risk of experiencing flooding, with six million of those individuals at risk of flooding that poses a risk to life and property (National Oceanic and Atmospheric Administration, 2020).

In recent years flood events in the Southeastern United States have become more frequent and caused increased economic loss as well as loss of human life (Alipour et al., 2020). The Intergovernmental Panel on Climate Change (IPCC) predicts that precipitation events will increase globally, potentially resulting in more flood events on rivers (IPCC, 2022). In addition to increased precipitation, increased human interaction with fluvial systems is likely in increase flooding (Yin and Li, 2001). After a large flood event in the United States that causes fatalities, people return to the area after the damage is cleared despite the risk associated with living in that location (Johanna et al., 2022). Similarly, in recent years floodplains and other flood-prone areas

have become more desirable places to live (Hemmati et al., 2020), increasing the potential for floods to impact people.

There are more than 8,500 active United States Geological Survey (USGS) streamflow gauges in the U.S., but only a relatively short flood history of the country is represented in the gauge record(United States Geologic Survey, 2020). In 1922 there were only 1,304 active streamflow gauges, which means that at most only ~15% of the gauges have records that extend beyond 100 years (United States Geologic Survey, 2020). Because of their relatively short time of operation, it is probable that most gauge records contain few, if any extreme floods (≥ 100-year flood) (England, et al., 2019). Because there are few observations of extreme floods for most river basins, flood frequency analysis of extreme floods produce estimates with a high degree of uncertainty (England, et al., 2019). This study sets out to identify when extreme flood events occurred on the French Broad River prior to the instrumental record and determine their magnitude so that they can be incorporated into future flood frequency analyses.

The Upper French Broad River, located in northeastern Tennessee is an excellent study site for reconstructing flood events because it is impacted by both large and small flood events caused by a number of factors and has a USGS gauge record that dates back to the 1860s. The construction of Douglas Dam on the French Broad River was completed in 1943 and is part of a larger flood control system protecting three downstream nuclear power plants, as well as numerous roadways, bridges, and water treatment facilities located in close proximity to the river (Tennessee Valley Authority, 2020).

1.2 Flood Frequency and Magnitude Changes

Paleoflood hydrology is a diverse field with a common goal: to reconstruct past floods and extend the length and number of flood observations, which is particularly beneficial to

understanding extreme flood hazards because of the dearth of large flood events in the instrumented record. Paleoflood studies are done by looking at physical evidence left behind by flood events (Benito and O'Connor, 2013). Evidence of floods can be seen and analyzed in a variety of different ways. Two archives of paleoflood evidence are sedimentological and tree-ring based (Anselmetti et al., 2020). Trees provide a wealth of information with regards to paleoenvironmental changes and disturbances, including floods. Debris transported by flood waters may cause external damage to a tree, which would leave a visible scar on the tree that could be used as a paleostage indicator (PSI) (Stoffel and Corona, 2014). The rings within trees can also provide information about flood activity. Trees can form and preserve "flood rings" if they are exposed to flood events during the spring growing season (Ballesteros-Cánovas et al., 2015). Sediments deposited by paleofloods (inland and coastal) can be found in lakes, floodplains, rock shelters/caves, speleothems, and in coastal ponds and beaches (Springer and Kite, 1997; Schillereff et al., 2014; Toonen et al., 2015; Denniston and Luetscher, 2017; Bregy et al., 2018).

Flood frequency and magnitude were significantly altered due to early human influences (Native American and European) in the southeastern United States (Rapuc et al., 2019). Euro-Americans began to settle in this region in the mid-1700's (Miller, 1969). During early colonization, there was large scale deforestation including clear cutting for agriculture by both settlers and to a lesser extent, Native American communities (McLauchlan, 2003). Clear cutting accelerates runoff and can increase flooding during precipitation events (Onda et al., 2010). If deforestation occurs along floodplains, this can lead to bank erosion, lateral migration of the river channel, as well as increased soil mobilization during precipitation events (Knox, 2006; Rapuc et al., 2019) creating more frequent and extreme flood events.

Global oceanic and atmospheric factors also impact flood frequency and magnitude. Sea surface temperature (SST) has a significant effect on streamflow across the entire United States (Tootle and Piechota, 2006; Sadeghi et al., 2019). Elevated SST is directly proportional to increased streamflow (Tootle and Piechota, 2006). These SST fluctuations are driven by Atlantic Multidecadal Oscillation (AMO), El Niño-Southern Oscillation (ENSO), and the Pacific Decadal Oscillation (PDO) (Tootle and Piechota, 2006). During the approximately 30-year positive phase of the AMO there is a significant hurricane risk to the southeastern United States (Curtis, 2008). Positive phases of AMO are linked to increased hurricane activity (Kashkooli and Modarres, 2020). While the AMO naturally fluctuates on a ~30-year cycle (Curtis, 2008), the Maunder Minimum (CE 1645 – 1715), which is a period of reduced solar activity, also has been shown to influence the AMO (Owens et al., 2017; Fang et al., 2019). During the Maunder Minimum, the northern hemisphere experienced the Little Ice Age (LIA), which has been linked as a direct result of solar influences on climate (Owens et al., 2017).

The northern hemisphere has also been subjected to several major climate anomalies during the Holocene. Most recently the LIA, which resulted in cooler temperatures in most of the northern hemisphere from ~1300 – 1900 CE (Rodysill et al., 2018; Lombardi et al., 2021). Prior to the LIA, the Medieval Climate Anomaly (MCA; ~800 – 1300 CE), was defined by significantly warmer temperatures in Europe and North America (Mann et al., 2009). Lombardi et al. (2021) showed that most extreme floods in Europe and North America occurred during the late MCA, while the highest frequency of flood events occurred during the LIA (Lombardi et al., 2021). Warmer periods bring severe droughts to the affected regions, as seen in Europe and North America during the early MCA (Rodysill et al., 2018). Since these periods are also very

prone to extreme flood events, it is possible that the conditions brought on as a result of drought are a precursor of extreme floods.

Several studies have looked at how flood frequency and magnitude have changed over the last century, however they do not incorporate floods that occurred prior to instrumental streamflow records (Pielke and Downton, 2000; Milly et al., 2002; Berghuijs et al., 2017; Blum et al., 2020; Alipour et al., 2020). Because instrumental records often do not capture the largest floods on rivers, we do not know if the frequency and magnitude of floods is changing over significantly longer periods. To determine if the frequency and magnitude of flood events is in fact shifting over longer periods, quantitative paleoflood studies are needed. Adding paleoflood information can significantly improve the estimates of the probability of a 100 year flood event (Hosking and Wallis, 1986; Reinders and Muñoz, 2021). Strupczewski and collogues determined that the shorter the gauge record the more useful historical information is for increasing the accuracy of flood frequency analyses (2014). Without information about the magnitude of paleoflood events, flood frequency analyses cannot be updated. Therefore, it is imperative that the magnitude component of paleofloods be derived.

1.3 Quantitative Paleoflood Hydrology

To help extend the record of past flood events, or paleofloods, one technique researchers use is quantitative paleoflood hydrology. Quantitative paleoflood hydrology is looking for and identifying PSIs, which are minimum estimates of paleoflood stage. Once these indicators have been identified, hydraulic modeling such as a 1D step-backwater model can be used to estimate a discharge associated with a specific PSI (Benito et al., 2022). Recently, new federal guidelines recommended that paleoflood hydrologic data be incorporated into flood frequency analyses to provide a more robust flood frequency analysis for low annual exceedance probability floods

(England, et al., 2019). Paleoflood data that can be used in updating flood frequency analysis must include indicators that can be used to quantify discharge data. These indicators are typically slackwater deposits (SWDs), such as cobble and gravel bars, or tree scars, and erosional scars (Ely and Baker, 1985; Springer and Kite, 1997; Jarrett and England Jr., 2002). Secondly, there should be some threshold information, which can include dated non-exceedance bound, which represents a flood stage that has not been exceeded over a known time period, and PSIs (England, et al., 2019). The period for which a flood has not exceeded a certain stage is determined by looking at stratigraphic and geomorphic evidence deposited by flood events. These deposits are then geochronologically dated to determine the specific period for the non-exceedance bound (Levish, 2002).

Only a handful of quantitative fluvial paleoflood studies have been conducted in the southeastern United States (Wang and Leigh, 2012; Leigh, 2018; Munoz et al., 2018; Harden et al., 2021a; Reinders and Muñoz, 2021). Most studies have focused on the southwestern United States because the field originally began by studying bedrock-valley reaches (Baker, 2008; Toonen et al., 2020). Studies in the southwestern United States have taken place at sites where there is little long term change of channel geometry through time (Benito and O'Connor, 2013) and where there is little bioturbation to disturb fluvial deposits. Leigh (2018) noted, however, that stable, bedrock morphologies do not exist in most places. He also points out that these bedrock gorges are typically not continuous and only capture the largest flood events (Leigh, 2018).

Other paleoflood studies that have been done in the southeastern United States, have shown what drives large flood events in the region, however few of these studies have determined paleodischarges. Wang and Leigh (2012), worked in the Upper Little Tennessee

River. Although they did not reconstruct discharge in their study, they did identify a decrease in the number of flood events during the LIA. Working in the Mississippi River, Munoz et al. (2018) found that flood hazard is inversely related to AMO, and more directly related to artificial channelization. As a result of river regulation, the magnitude of a 100-year flood event in the Mississippi River increased by 20% over the 500 year study period (Munoz et al., 2018). Additionally, by using lipid biomarkers preserved in lake sediments, flood and drought periods during the MCA were identified within the Mississippi River basin (Muñoz et al., 2020).

Paleoflood data can provide a wealth of information that is simply not available using only gauge records. In bedrock channels, combining paleoflood information with systematic information results in a significant decrease of uncertainty (Liu et al., 2020). In one study in a semi-alluvial channel incorporating paleoflood information into the flood frequency analysis resulted in a 50% reduction in uncertainty in the AEP of a 100-year flood event (Lam et al., 2017). Lombardi and Davis (2022) used quantitative paleoflood data from two sites in northern Alabama on the Tennessee River and reduced the AEP uncertainty by ~80% for the estimate of a flood with an AEP of 0.0001. By using sedimentary records, the magnitude and the frequency of flood events that were previously unquantified can be estimated and used to reduce the uncertainties associated with low AEP event predictions.

1.4 Study Objectives

This thesis reconstructs past extreme flood events that occurred on the French Broad River using overbank floodplain deposits and slackwater deposits preserved in rock shelters. Objectives of this research include: 1) extending the flood chronology of extreme events on the French Broad River beyond that of the instrumental and historical records 2) analyzing this extended flood record to determine if floods on the French Broad River have increased in

magnitude and frequency over both the instrumental record, as well as over longer time scales 3) identify drivers of the most extreme flood events on the French Broad River.

2. STUDY AREA

2.1 The French Broad

The French Broad River's headwaters are located in southern North Carolina near the northwestern border of South Carolina. The river flows northward through North Carolina and into northeastern Tennessee (**Figure 1**). The river continues to flow through northeastern Tennessee until it joins the Holsten River near Knoxville, Tennessee. These two rivers form the Tennessee River, which flows through much of southern Tennessee and northern Alabama. The French Broad River has a drainage area of 13,263.29 km^2 (WATERS, United States

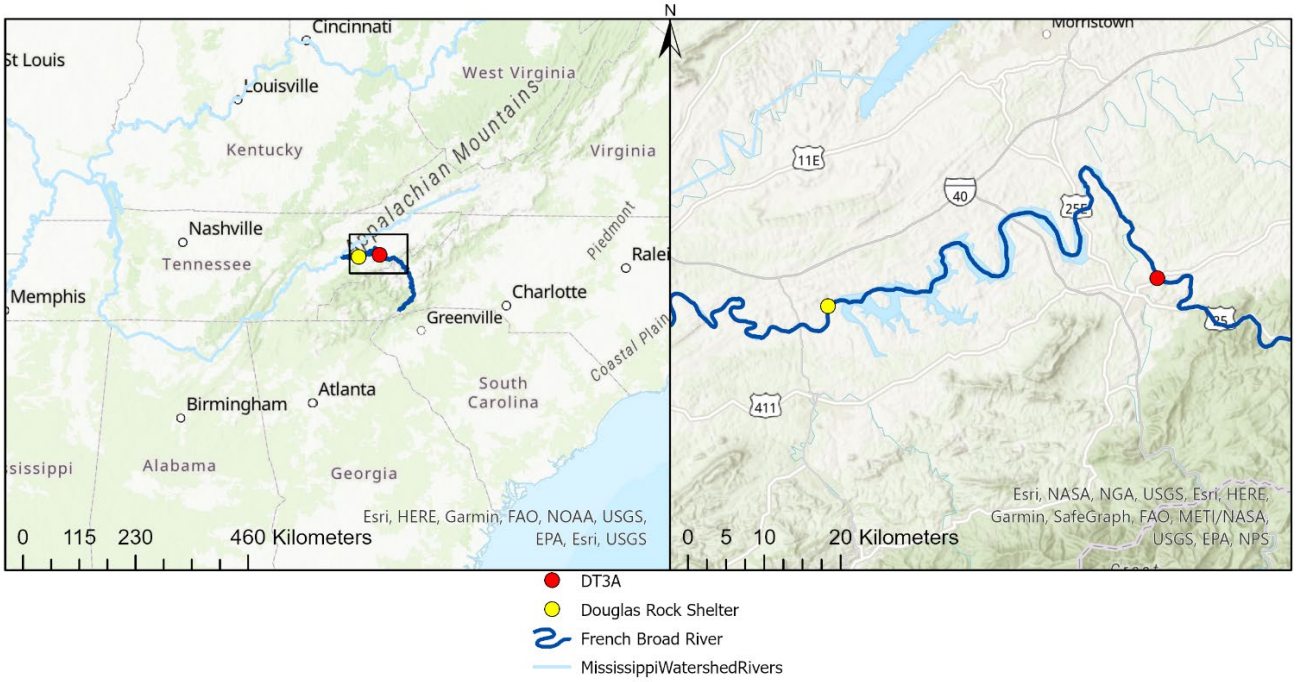

Figure 1: Map showing Douglas Terrace 3A (DT3A) and Douglas Rock Shelter (DRS) in relation to each other. These sites are located in northeast Tennessee near the North Carolina Boarder along the French Broad River. The two sites are separated by ~35 km.

Environmental Protection Agency, 2020). This makes the French Broad River the largest tributary of the Tennessee River (Tennessee Valley Authority, 1961).

The headwaters of the French Broad River primarily flow through a bedrock channel made up of metamorphic rocks in the Blue Ridge Mountains (Harden and O'Connor, 2017). These metamorphic rocks are rich in feldspar, mica (muscovite and biotite), and quartz (Huang and Wang, 2005). Because mica is the third most abundant mineral group in the watershed, it is an indicator of sediment deposition due to flood activity on the French Broad River, which makes flood deposits easily identifiable (Huang and Wang, 2005; Harden et al., 2021a). The bedrock transitions to sedimentary rock types as the river flows into northeast Tennessee (Lemiszki and Price, 2005).

2.2 Flood mechanisms and historical/historic floods

The Tennessee Valley is most susceptible to flood events from November through late March or early April (Tennessee Valley Authority, 1961). The USGS gauges at Newport, TN and below Douglas Dam (Kodak, TN) show February, March, and April have the highest mean discharges (USGS 03455000; USGS 03469000) (**Figure 2**).

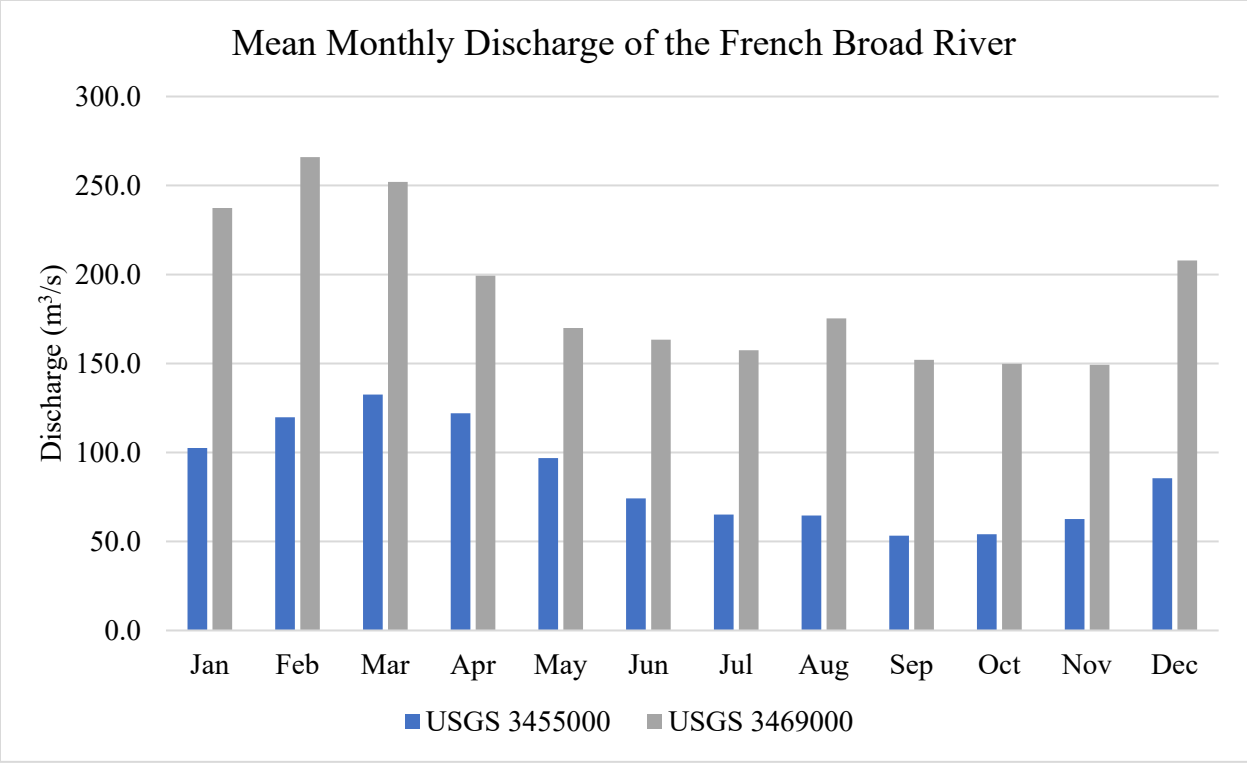

Figure 2: Plot of the mean monthly discharges at two different USGS gauge stations on the French Broad River. USGS 3455000 is located at the alluvial terrace site (DT3A), and USGS 3469000 is located at the rock shelter site (DRS).

Increased flooding during these winter months is caused by frequent widespread thunderstorms, while tropical storms, and mid-latitude cyclones that produce heavy precipitation result in flooding during summer and fall months (Tennessee Valley Authority, 1961). During the summer and fall, the French Broad drainage basin is particularly susceptible to precipitation produced by tropical cyclones moving inland from the coast (Tennessee Valley Authority, 1961). Flooding is more intense in the winter months because of normally high soil moisture content. During the warmer months in the French Broad watershed, water is being removed from the soil due to high evapotranspiration demand (O'Geen, 2007; Kim et al., 2019). Thus, when a large precipitation event occurs, water more readily infiltrates the soil and may not cause flooding until the soil has reached its capacity.

Currently, the flood of record for the French Broad River is the flood of 1876 (Tennessee Valley Authority, 1940). This flood had a discharge of ~3,114.85 m^3/s ((Tennessee Valley Authority, 1940), USGS 03455000). There are two other flood events that had similar discharges and stages. The 1902 and 1916 floods had discharges of 2,860.00 m^3/s and 2,746.73 m^3/s respectively (USGS 03455000). A Tennessee Valley Authority (TVA) report from 1961 describes several large flood events on the French Broad River. The largest and earliest known flood occurred in July 1791, and was caused by non-tropical precipitation (Tennessee Valley Authority, 1961). The flood of August 1796, May 1845, and August 1852 are also mentioned in this document as being larger than the flood of August 1928, which had a discharge of 1,257.27 m^3/s (Tennessee Valley Authority, 1961) (USGS 03455000). These three floods are described as being "freshets" (Tennessee Valley Authority, 1961). The term "freshet" is defined in the report as precipitation resulting from a hurricane event (Tennessee Valley Authority, 1961).

2.3 Site selection

Data for this thesis were collected from an alluvial terrace (DT3A) and a rock shelter site (DRS1) along the French Broad River, near Douglas Lake and Douglas Dam. These sites are located in Newport and Kodak, Tennessee respectively (Figure 1).

2.3.1 Douglas Terrace 3A site

Site DT3A was chosen because of its proximity (roughly 100 meters downstream) from an exceptionally long USGS gauging station with ~150 years of observations. This station (USGS 03455000) has reconstructed streamflow and water surface elevation data for the flood that occurred on March 7, 1867, making it one of the oldest gauges in the United States. It also contains stage recordings for numerous additional historical flood events that occurred on the French Broad River (United States Geologic Survey, 2020) (**Figure 3**). The gauge has a more

continuous measured record beginning in 1901 and continuing through present day (USGS 03455000). The 1867 flood is reported to not have impacted the DT3A site, however a flood that is described as having a very similar discharge in 1876 is recorded as impacting the DT3A site (Tennessee Valley Authority, 1940).

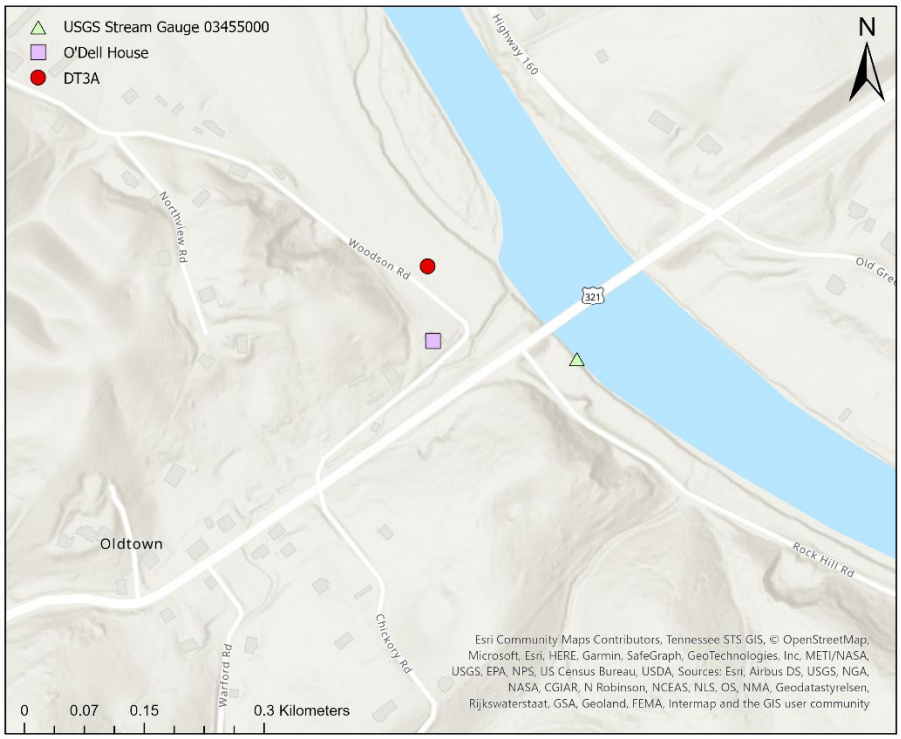

Figure 3: Map showing the location of the DT3A site where the sediment core used for this study was taken. The USGS gauge station 03455000 is also shown.

2.3.2 Douglas Rock Shelter (DRS) Site

The DRS site is located in an alluvial-bedrock gorge approximately 1 km downstream of Douglas Dam and ~35 km downstream of DT3A. This site is impacted by both the 1867 flood and the flood of 1876 due to it being downstream of Dandridge, Tennessee which recorded both floods having nearly identical magnitudes (Tennessee Valley Authority, 1940). The top of the canyon walls are approximately 30 m above the river which runs through the middle of the

gorge. From the channel margin to the base of the slope of the wall is a floodplain that is on average 45 m in width and runs continuously downstream on both sides of the river. The hillslopes are made of limestone which contain alcoves and rock shelters. The NRCS defines the soil located from the ridge to the river's edge as Combs, which is characterized by frequent fluviomarine deposits, as well as being frequently flooded (NRCS, 2021). The soil on top of the ridge where the rock shelters are located is defined as Talbott and Rock outcrop (NRCS, 2021). Talbott soil series is part of the alfisol order, which is made up of clay that has been weathered from the limestone beneath (NRCS, 2021). While these soil profiles are present above and below the rock shelters respectively, most of what is expected to be found in the rock shelters are fluvial deposits and break down of the rock shelters themselves.

Three rock shelters were identified at the DRS site. DRS1A, is the lowest rock shelter with an elevation of 276.0 m asl. The mouth of the shelter is ~3 meters tall and ~2 m wide. There is a large limestone boulder at the entrance that is ~1 m by ~1.5 m. We dug a 24 cm deep test unit (DRS1A-MD) between the boulder and the southwest wall of the shelter.

The next rock shelter, DRS1B, has an elevation of 279.7 m asl and is located downstream of DRS1A. This rock shelter has a mouth that was ~1.5 m tall and 2 m wide. The shelter extends ~4.5 m inward from the mouth. We dug an 18+ cm deep test unit (DRS1B-BP) in the southern corner of the shelter. Finally, DRS1C is the highest of the three shelters, with an elevation of 287.3 m asl (**Figure 5**).

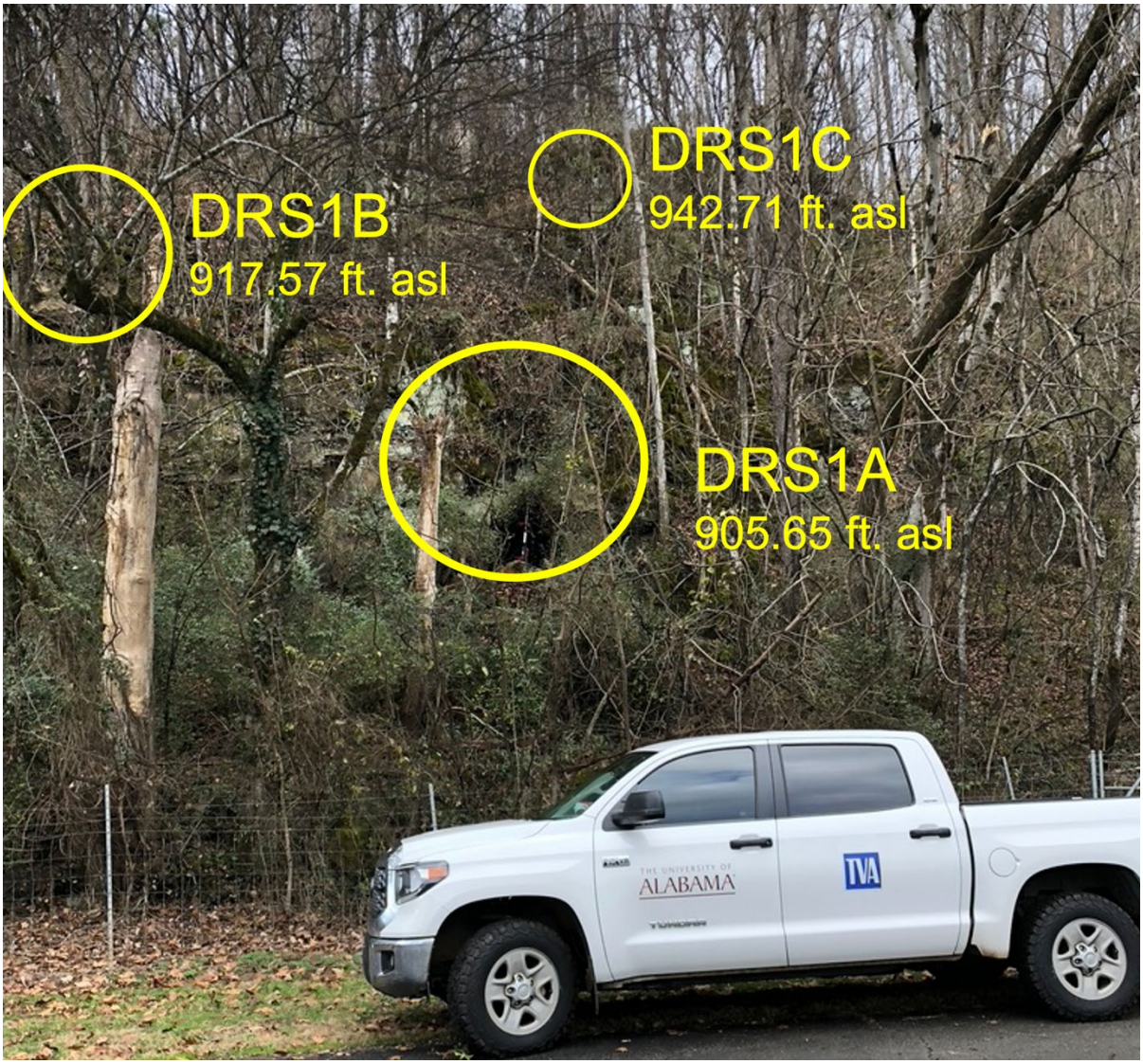

Figure 4: Locations and elevations of the three Douglas Rock Shelters

The two sites are located 35 km from each other, with DT3A being the upstream site. The area that drains through the DT3A site is 4,801.651 km^2, while the area for the DRS site is 11,785.375 km^2 (WATERS, Environmental Protection Agency, 2020). The drainage area of the DRS site is significantly larger than that of the DT3A site because it is located downstream of where the Pigeon and Nolichucky Rivers flow into the French Broad River. The area of the basin upstream from DT3A makes up 40.7% of the total area that drains to the DRS site. Combined,

these sites account for 88.9% of the total drainage area for the French Broad River. This can be seen in **Figure 4**. Soils at DT3A include sandy to silty loams (Biltmore and Bloomingdale Series) that are occasionally ponded (NRCS, 2021). These soils sit on top of sedimentary rocks primarily composed of limestone and dolostone (Hardeman et al., 1966). The soil information indicates that the area is often flooded by the river, and during these flood events, sand and silt are deposited forming slackwater deposits as noted by Ely and Baker in other parts of the United States (NRCS, 2021; Ely and Baker, 1985). This type of fluvial deposit is crucial for reconstructing paleofloods.

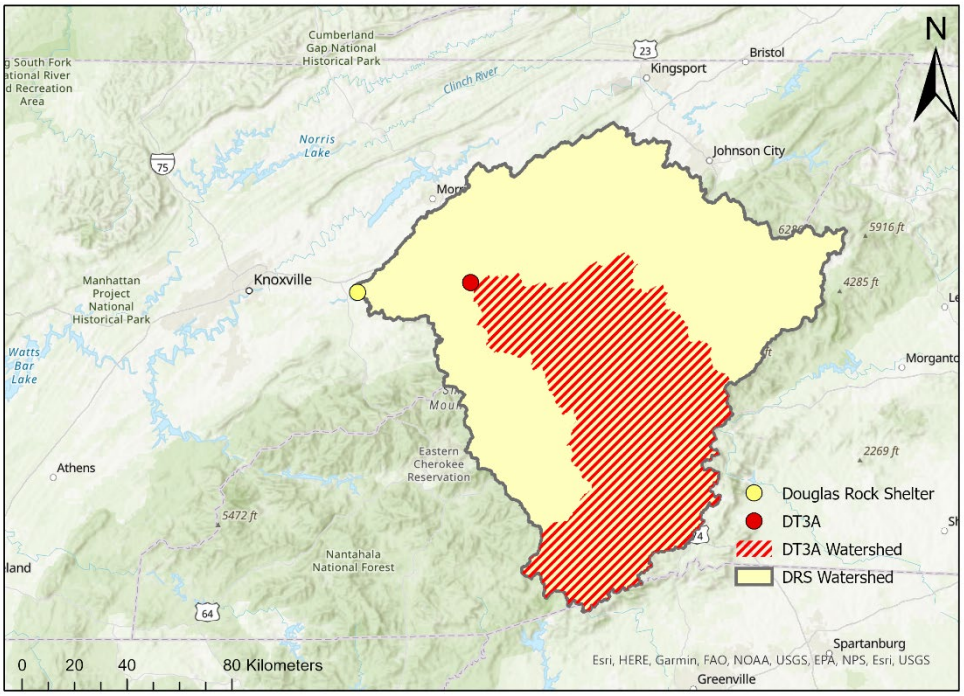

Figure 5: Map of the drainage area that flows through the Douglas Terrace 3A site and the Douglas Rock Shelter site. The area in yellow is the drainage area of DRS. The red hatched area is the drainage area of Douglas Terrace 3A site. This red area also flows through the DRS site. The total drainage area for DRS is 11,785.375 km^2.

3. METHODS

3.1 Paleoflood chronology alluvial terrace site

In January 2021, we pulled twin cores from the DT3A site. One core was used for particle size analysis (PSA), loss on ignition, and radionuclide dating, we used the other sediment core for optically stimulated luminescence (OSL) dating. The liners used for the OSL core were painted black to prevent bleaching of the sediment when they were extracted from the ground. These cores were collected using a hydraulic coring rig operated by Technical Drilling Services from Knoxville, AL. The maximum depth of the bore hole was measured once there was refusal from hitting rocks under the floodplain. The cores were sealed and transported back to The University of Alabama for analysis.

For PSA (DT3A) we split, described, and sampled core DT3A at a resolution of 1 cm down the length of the entire core. We added to each of the 163 samples taken, 200 mL of a 50g/L solution of sodium hexametaphosphate. This acts as a deflocculant. We allowed the solution to sit overnight before PSA. We measured the particle size of each sample using laser granulometry. We used a Bettersize Bettersizer S3 Plus to measure PSA.

Once we analyzed all 163 samples, the data were exported into 100 bins based on each sample's φ scale grain size. This is done so that the end-member model (EMMA) can compare different subsamples of grain size and is used to identify the geomorphic processes responsible

for the deposition of the end members (Toonen et el., 2015). This end member analysis is done using the R package *EMMAgeo* (Dietze and Dietze, 2019).

A change point analysis (CPA) was then performed on end-member 1 and 2, identified from the EMMA (Toonen et al., 2015). This change point analysis is also done in R using the *changepoint* package (Killick, 2016). This package identifies any major changes in sedimentation rate throughout the length of the sediment core.

After the CPA, we applied a locally weighted smoothing regression model (LOESS) to the sand fraction of the particle size data using R (Leigh, 2017). From the LOESS smoothing, the positive residuals were identified, which represent flood deposits captured in the sediment core.

Several different types of dating techniques were used to determine the age of the sediments collected in the core. One dating technique that was used was radiogenic dating. Radiogenic dating measures the concentrations of ^{210}Pb and ^{137}Cs concentrations in the sediment. ^{210}Pb and ^{137}Cs are isotopes that are particularly useful in dating young sediment. This is where other dating techniques fail to provide accurate dates (Nittrouer et al., 1979; Leigh, 2017). These two isotopes are largely produced by anthropogenic sources (i.e. leaded gasoline and nuclear fallout) where they then bind to organic rich material that holds them in the soil profile (Abbasi, 2019). Samples were extracted at 5 cm increments from the DT3A core. The samples were weighed and sent to Flett Lab LLC for radiogenic dating.

Optically stimulated luminescence (OSL) was used to date older sediment from the core. It is particularly useful to date quartz and feldspar rich minerals. OSL can provide dates for the last time that sediments were exposed to sunlight (bleached), which is assumed to be approximately the same time that the sediments would have been deposited by a flood event (Nelson et al., 2015). This technique has been used in fluvial settings and works well as long as there is

sufficient quartz and feldspar material to date and that they have been completely bleached during a flood event (Rittenouer, 2008). To date sediment from the DT3A core, the core was split under red light. Areas of interest were identified, and samples were cut with a buffer of 10 cm on either side. These were packaged and sent to the Utah State University Luminescence Lab.

Due to frequent sediment deposition the residency time of these sediments could not be established on the French Broad River, and therefore a constant sedimentation rate could not be assumed. To remedy this a Bacon age depth model (ADM) was constructed with the ^{210}Pb, ^{137}Cs, and OSL dates using the package *rbacon* in R (Blaauw and Christen, 2011). The Bacon age model produces a sedimentation rate, as well as age estimates of deposition using Bayesian statistics and a Student's t-distribution, respectively (Blaauw and Christen, 2011; Bregy et al., 2018). For this model, the boundary function was used instead of the hiatus function. The boundary function is used to indicate major stratigraphic changes, that do not necessarily constitute a hiatus (Blaauw and Christen, 2011). These boundaries were identified by C horizons within the sediment core. In its entirety, the DT3A core looked as if it was one large A horizon that was interrupted by flood deposits (C horizons). A sensitivity analysis was done on the ADM by running several iterations of the model. The first only used the following C horizons from the DT3A core: U1, U7, U17, and U26. These horizons are the thickest within the core. The next iteration included U9, U12, and U22 in addition to the previous units from the first run. The second run provided dates that were more in line with what was expected based on the OSL, ^{210}Pb, ^{137}Cs, and dates of nails from the test unit.

3.2 Paleoflood chronology rock shelter site

Two trips were made to the Douglas Tailwater (DT) site. During these trips, three rock shelters were identified. These rock shelters were determined to be significant for identifying and dating large paleoflood events. These large paleoflood events have deposited sediment and other material in the lower two rock shelters at the DT site. Additionally, these sites were surveyed by a registered land surveyor from the TVA and measurements of the entrances of all three rock shelters were measured with sub-centimeter accuracy.

In the lowest rock shelter, Douglas Rock Shelter 1A (DRS1A), we dug a small pit (DRS1A-MD) between a large boulder in the center of the shelter and the southwest wall. This pit was named the Mt. Dew pit because fragments of a glass Mt. Dew bottle were found near the surface. Before digging, cave breakdown was removed from the surface. This breakdown was made up of < 10 cm rocks. Once cave breakdown was removed, we dug a 30+ cm deep pit and described it. When surveyed, the mouth of DRS1A was at an elevation of 276.0 m asl.

3.3 Paleodischarge estimates

The most common method of determining paleodischarges is by using a steady flow step-backwater method to model the discharges (Webb and Jarrett, 2002; Maharjan and Shakya, 2016). To determine the discharges of paleoflood events, a step-backwater model was built. This model generates water surface elevations for specific discharges (O'Connor and Webb, 1988; Yang et al., 2022). Using the water surface elevation obtained from the step-backwater model, a minimum estimate of the discharge of a paleoflood can be determined based on the elevation of paleostage indicators (Margold et al., 2018; Yang et al., 2022). The step-backwater model

requires specific information about the system to be accurate. This includes channel geometry, hydraulic properties, and channel slope (Webb and Jarrett, 2002). The model built for this project, used LiDAR imagery with a resolution of 1 meter, that was provided by the TVA. One-dimensional models are the most common type of step-backwater model because, for multidimensional models, significantly more data is needed to build the model (Webb and Jarrett, 2002; Margold et al., 2018; Victoriano et al., 2018; Yang et al., 2022). A steady flow is assumed in the model because for each iteration, the discharge was remaining constant (Maharjan and Shakya, 2016; Harden et al., 2021b). The U.S. Army Corps of Engineers Hydrologic Engineering Centers River Analysis System (HEC-RAS) was used to create the model (USACE, 2022). HEC-RAS is the most common program used for step-backwater modeling because it is able to model any system provided sufficient data is input (Webb and Jarrett, 2002; Maharjan and Shakya, 2016; Harden and O'Connor, 2017; Margold et al., 2018; Harden et al., 2021a).

3.4 Rock shelter site paleodischarge estimates

The TVA provided an extensive HEC-RAS reconstruction of channel geometries for the French Broad River, and these channel geometries, with some modifications, were the basis of the DT site's hydraulic modeling. Modifications to the base HEC-RAS model included removing modern features of the river (Douglas dam, lateral structures, and other rivers) not relevant to the DT study site and adding a cross-section where cross-sections were lacking in the original TVA HEC-RAS channel reconstructions.

Upon examination of the cross sections, which are numbered sequentially as river stations (RS) based on their corresponding river mile (**Figure 6**), it was apparent that there was not a cross section near the DRS1A and B study sites. For this study a resolution of at least two cross sections per river mile was desired. This spacing was created by importing a DEM that was provided by TVA, into HEC-RAS. From this DEM data, a new cross-section at the exact location of DRS1A and B was drawn in the RAS Mapper tool built into HEC-RAS. This cross section that was created is labeled RS 31.120 in **Figure 6**. River station 31.120 was the primary

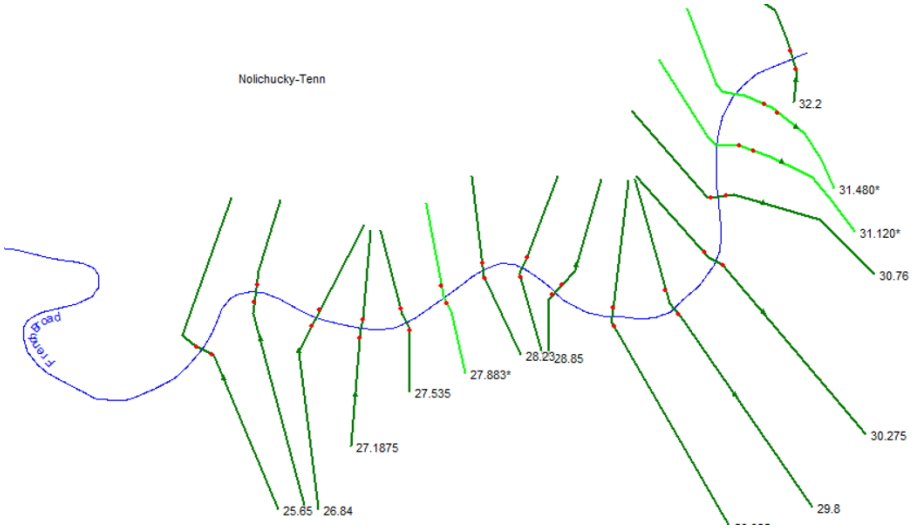

Figure 6: French Broad River with cross sections. DEM data was provided by TVA. RS 31.120 was created at the location of the DRS1 site.

cross-section used when inputting discharges into the HEC-RAS model used to estimate paleodischarges.

The profile of this cross section was then extracted in ArcGIS Pro to verify that the cross section is representative of what was seen while doing fieldwork. The profile for this cross-section is shown in **Figure 7**. It was determined that the profile of RS 31.120 was representative of the topography that was observed during fieldwork.

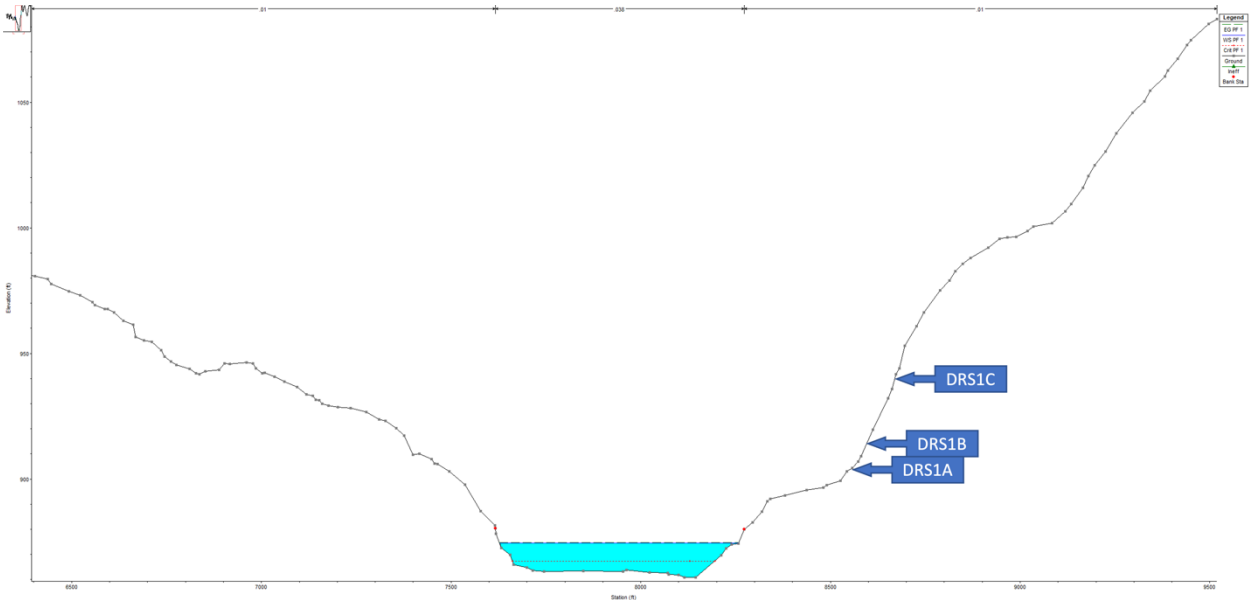

Figure 7: Cross section 31.120 which is located at the DRS site. The three rock shelters at DRS are highlighted at the correct elevation.

3.5 Hydraulic model calibration

The frictional slope for the model was calculated by measuring the slope of the 1867 flood from the TVA profiles of high-water marks from 1941 (before the construction of Douglas Dam). The slope was calculated to be 0.0004735 m/m. This slope was used for all subsequent calculations and iterations of the model. To calibrate and determine how accurate this frictional slope is, three of the largest floods of record were run through the model. The first was the 1867 flood. Based on the TVA Flood Profiles, this flood reached a height of 273.41 m asl at the DRS sites. HEC-RAS determined the height of this magnitude of flood to reach a height of 271.20 m asl. This is a difference of 2.21 m. This is however an approximate value because the discharge was calculated and not directly measured. The next flood that was used to calibrate the model was the 1916 flood which had a discharge of 3228.12 m^3/s. The TVA flood profile indicates that this flood reached a height of 272.49 m asl at the DRS sites, while HEC-RAS calculated that the height would be 270.72 m asl. This is a difference of 1.77 meters. Finally, the flood of 1940 was

input into HEC-RAS. This flood had a discharge of 2160.58 m^3/s and reached a height of ~270.6 m asl. HEC-RAS determined the height of a flood of this magnitude to reach a height of 269.87 m asl. This is a difference of 0.80 meters.

Next, it was determined the magnitude of flood required to reach DRS1A and B. The heights of these rock shelters are 276.04 and 279.68 m asl, respectively. To reach DRS1A a flood would need a discharge of at least 8,155.25 m^3/s. A flood of this magnitude would have a water surface height of 276.06 m asl. For DRS1B a discharge of 13,110.70 m^3/s is required for the water level to reach the cave. This flood would have a water surface height of 279.76 m asl.

Non-exceedance bounds were identified and dated at both DRS and DT3A sites, however in both cases the dates that were obtained from the pits were modern and did not provide any useful additional data. For this reason, they were not considered in the interpretations and instead positive evidence of flooding was what was considered.

Finally, a sensitivity analysis was conducted on the roughness coefficient of the floodplain and channel's, Manning's *n*, as well as the slope (Li et al., 2014). The sensitivity analysis was done to determine the robustness of the model by examining the extent of which the results change when input values are adjusted, which shows how dependent the results are on certain variables (Thabane et al., 2013). The value of *Manning's n* is highly variable and depends on several factors including surface roughness, vegetation, channel irregularities, channel alignment, scour and deposition, obstructions, size and shape of the channel, stage and discharge, seasonal changes, temperature, and suspended material and bedload (USACE, 2022). The variability in *Manning's n* makes it a possible source of error in the calculations for discharge based on sediment deposition. *Manning's n* is used in the following formulas by HEC-RAS to

help calculate the total conveyance and velocity coefficient, which are required to determine the discharge.

$$Q = KS_f^{1/2} \qquad \textbf{Eqn. 1}$$

$$K = \frac{1.486}{n} AR^{2/3} \qquad \textbf{Eqn. 2}$$

$$Q = \frac{k}{m} AR^{\frac{2}{3}} \sqrt{S_f} \qquad \textbf{Eqn. 3}$$

Where K is the conveyance, n is Manning's roughness coefficient (*Manning's n*), *A* is the flow area, *R* is the hydraulic radius (area/wetted perimeter), and S_f is the frictional slope (Chow, 1959; Harden et al., 2021; USACE 2022).

HEC-RAS breaks up the river system into three areas: left bank, channel, and right bank. All three of these can have unique *Manning's n* values. However, this sensitivity analysis assumes that the left and right banks are the same. Arcement and Schneider (1989) published a paper titled "Guide for Selecting Manning's Roughness Coefficients for Natural Channels and Flood Plains" through the USGS. This paper has several tables that outline what the value of Manning's roughness coefficient should be based on the physical properties of the channel and the floodplain. While this guide is invaluable for determining the value of the roughness coefficient, field observations are most important for determining the value.

The values that are traditionally used for the Manning's roughness coefficient in the Upper Tennessee River watershed are 0.1 for the banks, and 0.035 for the channel. The discharges for of the floods of 1920, 1935, and 1936 flood were used for all the sensitivity analyses. The Manning's n values were adjusted +/-25% to see the impact of changing each

parameter. In total, seven runs were done while varying the parameters of the Manning's roughness coefficient. To determine the effect these variations had on the model, the percent difference between the hydraulic channel depths were compared to the original values. These hydraulic channel depths were determined using the unchanged Manning's roughness coefficient and the original slope. At most the adjustments caused a 16% difference between the two.

Based on the vegetation at the site, the original value of 0.1 was determined to be sufficient for representing the roughness coefficient of the floodplain. The results from these sensitivity analyses can be seen in **Table 1**.

The model was also run with the slope being 25% higher and lower than the calculated value. Increasing the slope by 25% resulted in a percent difference from the standard of -0.88%, 0.73%, and 0.78% for the floods of 1920, 1935, and 1936 respectively. Lowering the slope 25% resulted in a percent difference of 1.56%, 1.40%, and 1.46% for the same flood events. These results can also be found in **Table 2**. Based on the three sensitivity analyses carried out, the slope is the most impactful to the model. This is because slope is used in several hydraulic equations, which allows the impact to compound over the use of the equations.

Table 1: Results from the sensitivity analysis of Manning's n, where the shaded area are the original values, and the unshaded area the hydraulic channel depths once the values are adjusted +/- 25%

	Flood Years		
	1920	1935	1936
Original Hydraulic Depths (ft)	20.47	17.88	19.16
Hydraulic Depth when Floodplain Manning's n is adjusted +25% (ft)	20.54	17.93	19.22
Hydraulic Depth when Floodplain Manning's n is adjusted -25% (ft)	20.35	17.82	19.08
Hydraulic Depth when Channel Manning's n is adjusted +25% (ft)	22.93	20.18	21.54
Hydraulic Depth when Channel Manning's n is adjusted -25% (ft)	17.52	15.05	16.28
Hydraulic Depth when Channel and Floodplain Manning's n is adjusted +25% (ft)	23.06	20.27	21.65
Hydraulic Depth when Channel and Floodplain Manning's n is adjusted -25% (ft)	17.47	15.03	16.24

Table 2: Results from the sensitivity analysis of slope, where the shaded area are the original values, and the unshaded areas are the percent difference on the hydraulic channel depth.

	Flood Years		
	1920	1935	1936
Original Hydraulic depths (ft)	20.47	17.88	19.16
Hydraulic Depth when slope is adjusted + 25% (ft)	20.29	17.75	19.01
Hydraulic Depth when slope is adjusted - 25% (ft)	20.79	18.13	19.44

4. RESULTS

4.1 DT3A stratigraphic evidence of flooding

Multiple flood units were preserved within the DT3A sediment core. Within the 163 cm core, 29 unique stratigraphic units were identified and described (**Figure 8**). These units show very little soil development, which is indicative of frequent flooding (Zielhofer et al., 2009). This unit contains slightly less sand than the above or below units, which also points toward this being a period of less active flooding. The final piece of evidence that suggests that this period was not one of active flooding is the presence of small flecks of charcoal imbedded in the unit. This indicates that there was likely a stable surface where people were able to build fires and inhabit the land without threat of being driven out by a flood for some period of time (Graves et al., 2019). The contacts of the units above and below are very easily identifiable due to the significant increase in the amount of sand in those units. Since there are no other segments of the core where there is significant soil development, it is likely that the area where this core was taken was very prone to flooding. This is evident by much of the third push from the sediment core, where there are 18 units within a 63 cm section. These sections alternate between light brown sandy units with little organic matter to units that have a darker color and have an increase in the clay and silt content. This again shows that soil development is beginning, until a flood occurs and deposits a new layer of material, restarting the soil development process. It can also be seen that the contacts are very abrupt in much of the core. This indicates that there was little transition time between the period of soil development and the deposition of new material, which is what is expected during flood events. Overall, this core provides an excellent glimpse into how

well this site is connected to the French Broad River due to the constantly aggrading nature of the core.

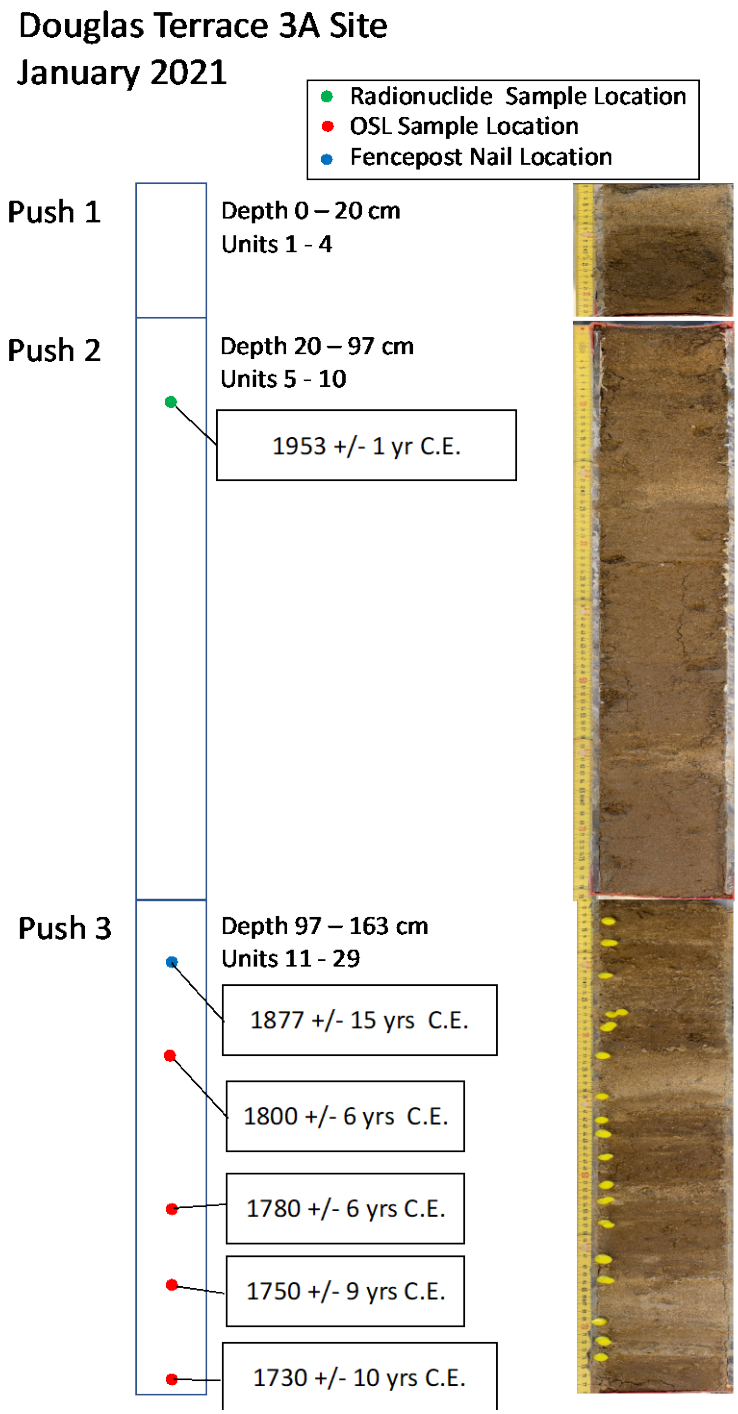

Figure 8: Stratigraphic details of the DT3A core, showing the pushes, the depths of the pushes, the units within the pushes, and the location from which dating materials were taken.

4.2 Floodplain site

Once all samples were analyzed using laser granulometry, the data were exported into 100 bins based on each sample's φ scale grain size. This is done so that the end-member model can compare the different subsamples of grain size. Three unique endmembers were identified (**Figure 9**). The lower right-hand plot of Class [φ] and relative amounts shows that EM1 is

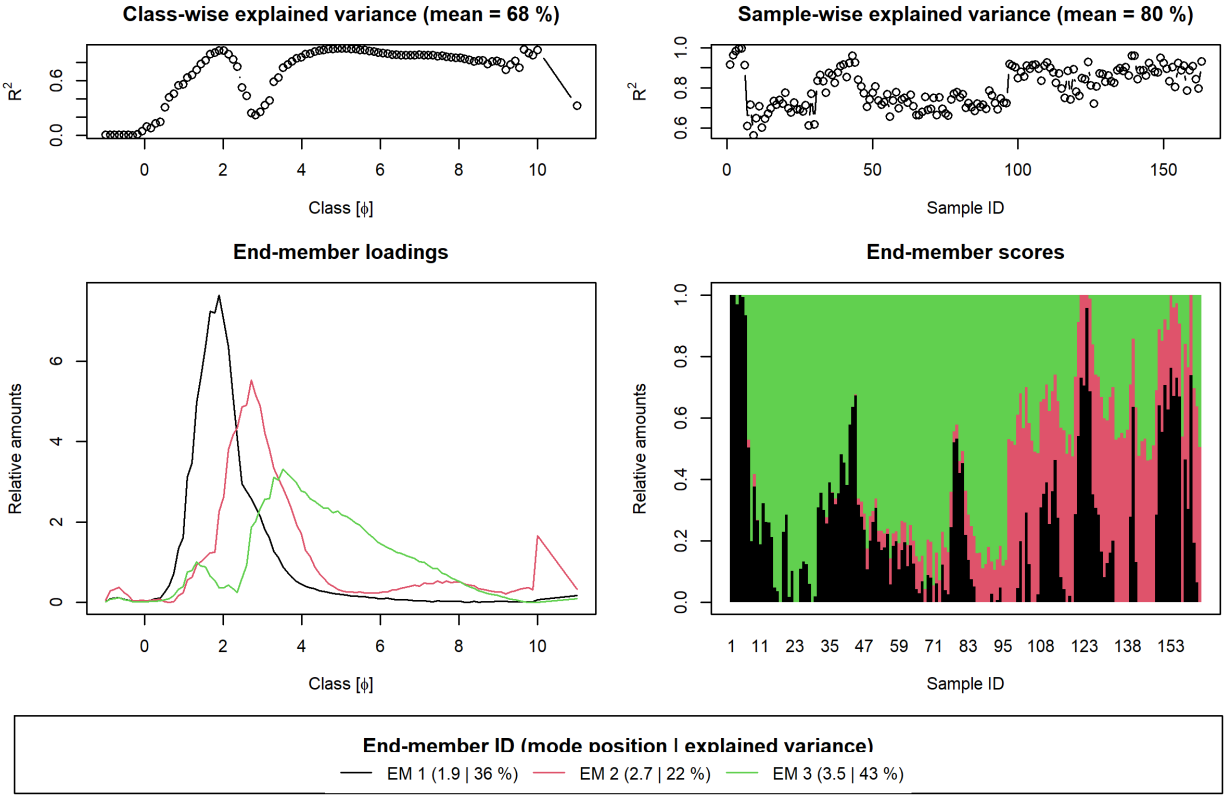

Figure 9: The results of the end-member modeling that was done using EMMA package in R.

primarily made up of medium to coarse sand (1.9 φ). This is attributed to large flood events that have been preserved in DT3A. The second endmember (EM2) is made up of finer sand (2.7 φ) and is likely explained by deposits from smaller flood events that have occurred within the core.

Finally, EM3 is representative of the very fine sand and silt populations (3-8 φ). The volume of sand was then isolated from the particle size data to continue the analysis. This particle size fraction includes both EM1and EM2, since these end-members both contain sediment deposited by floods. A change point analysis was then performed. The CPA showed zero change points, which indicates that the entire core is from an active flood period. A locally weighted smoothing regression model was then applied to the sand fraction of the particle size data (**Figure 10**). From this LOESS smoothing, the positive residuals were identified and are plotted in **Figure 11**. These positive residuals are attributed to flood events.

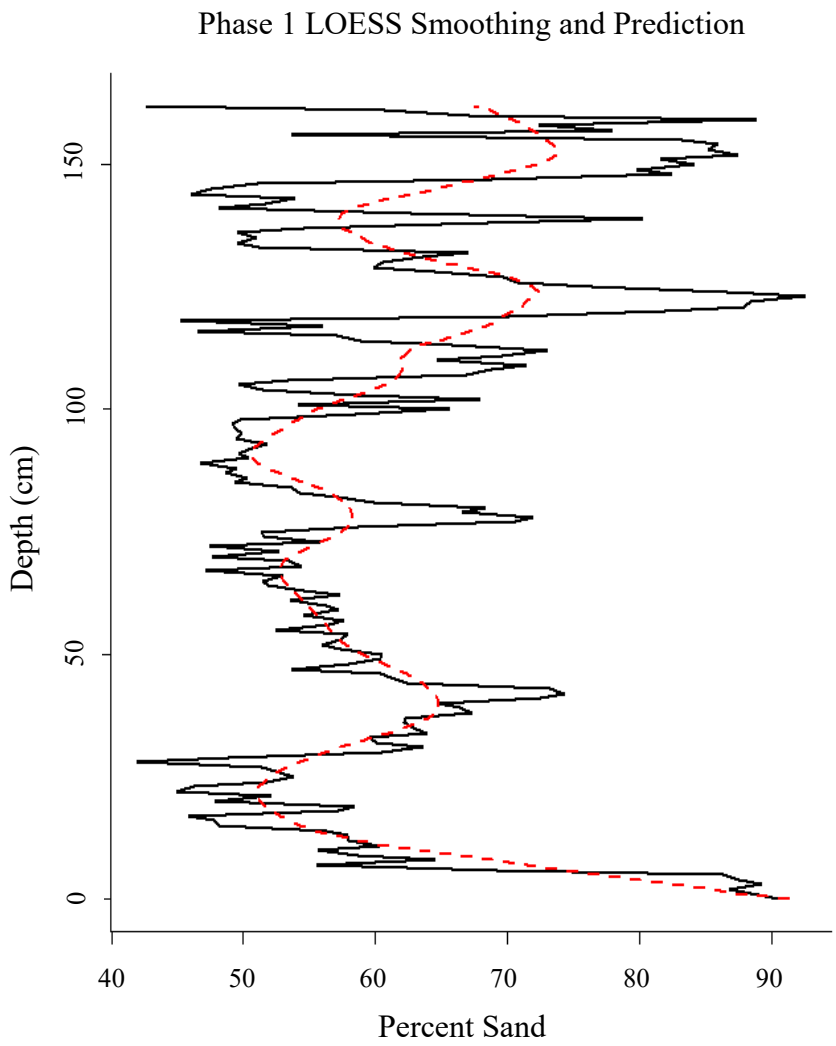

Figure 10: The locally weighted smoothing regression model carried out on the PSA data from DT3A sediment core. The smoothed line is shown as the red dotted line and everything above the smoothed line is a positive residual.

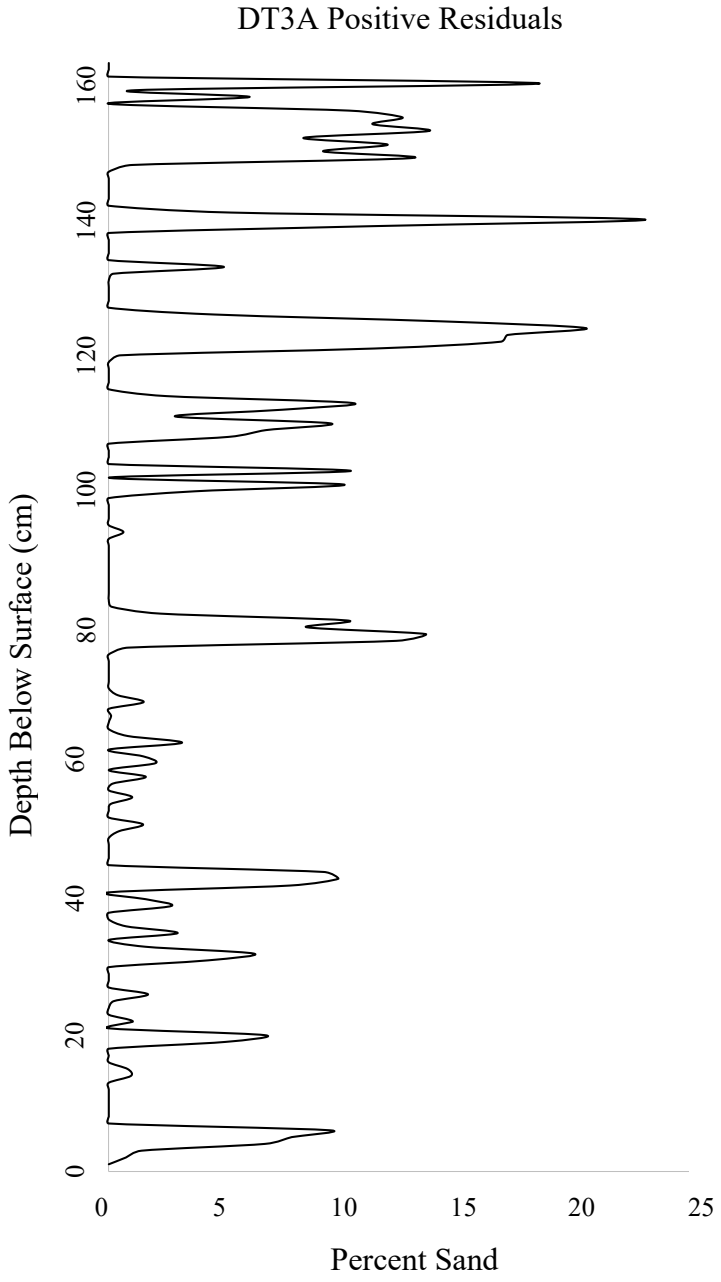

Figure 11: The peaks in the volume of sand above the LOESS trendline from DT3A

To construct the age depth model, dates that corresponded to specific depths were needed. The ^{210}Pb activity within the core pulled from DT3A suggests that sediments below a depth of 29.25 cm are older than 1953 C.E. Analyzing the DT3A core for ^{137}Cs showed that

sediments below 25 cm were deposited before 1963 when nuclear testing began. OSL dating was able to provide dating information for the bottom section of the sediment core. The depths of the OSL samples and the corresponding dates are shown in **Table 3**.

Table 3: List of depths of OSL samples and the corresponding data as well as the dates that were determined by the USU Luminescence Laboratory

Sample ID	USU ID	Depth (cm)	Percent Water Content	Total Dose (Gy/kyr)	Equivalent Dose (Gy)	Overdispersion (%)	Date (years before 2020)
DT3A-OSL-U17	USU-3720	120	10	3.11 +/- 0.12	0.69 +/- 0.24	66 +/- 9	220 +/- 6
DT3A-OSL-U22	USU-3721	139	14	3.24 +/- 0.13	0.79 +/- 0.34	69 +/- 13	240 +/- 6
DT3A-OSL-U26/26	USU-3722	148	8	2.88 +/- 0.11	0.78 +/- 0.34	65 +/- 10	270 +/- 9
DT3A-OSL-U28	USU-3723	158.5	10	3.05 +/- 0.12	0.89 +/- 0.48	53 +/- 15	290 +/- 10

By inputting the above dates into the R package "rbacon", an age depth model was constructed (Blaauw and Christen, 2011). The result of the ADM is shown in **Figure 12.** The ADM determined that the mean age of the bottom of the 163 cm DT3A sediment core is 295 years before 2020. Combining this ADM with the positive residuals provides the dates of the large flood events that correspond with the positive residual plot. This combined plot is shown in **Figure 13**. The largest 20% of positive residuals are identified in **Figure 13**, which are considered the most extreme flood events within this reconstructed record.

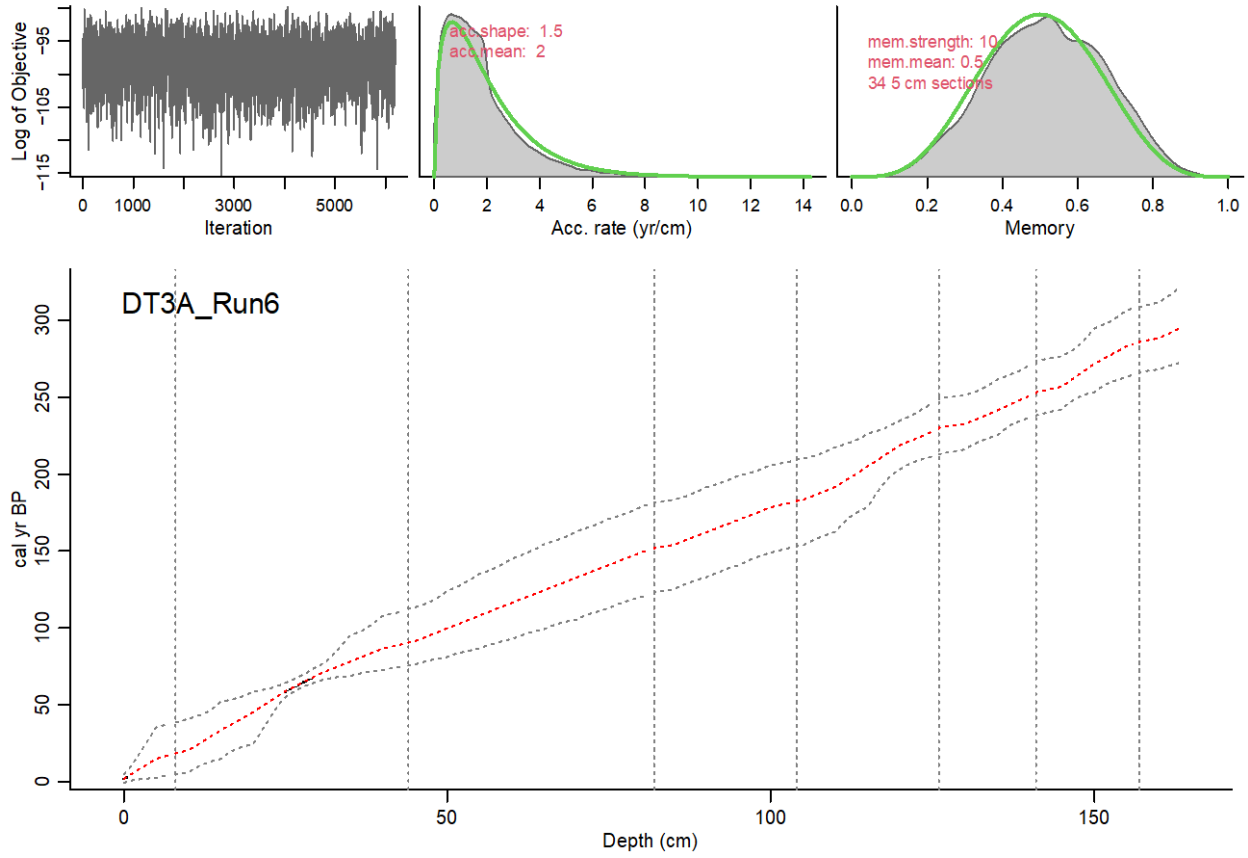

Figure 12: Results of the "rbacon" ADM using OSL, 210Pb, and 137Cs, and in situ nail dates as inputs (Blaauw and Christen, 2011).

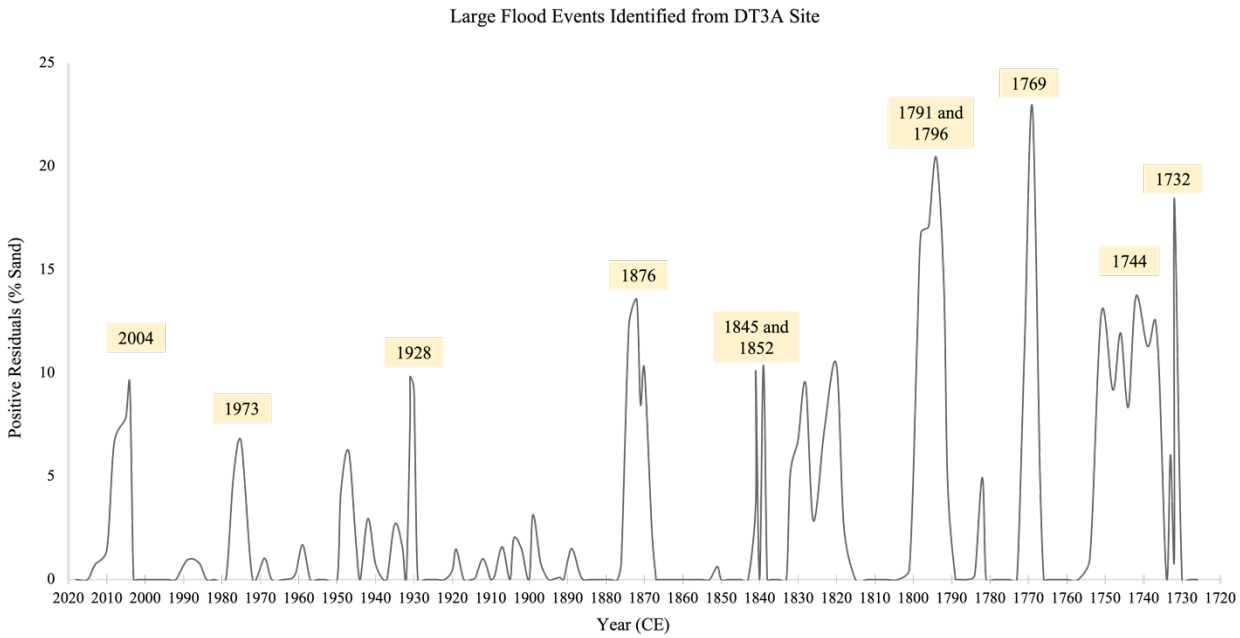

Figure 13: Sand peaks above LOESS trend line from DT3A. These peaks represent one or more paleoflood events occurring within a 30-year timespan.

4.3 Rock Shelter

Based on the stratigraphy of DRS1A-MD, unit 2 was determined to be a flood deposit. The flood unit was identified because mica was absent from units 3 and 4. This indicates that there was a large flood that deposited mica in the cave on top of unit 3. To determine the approximate age of the flood that deposited the mica in DRS1A, several charcoal samples were taken from different stratigraphic units in the pit.

Based on the stratigraphy of DRS1A-MD (**Figure 14**), unit 2 was determined to be a flood deposit. The flood unit was identified because mica was absent from units 3 and 4. This indicates that there was a large flood that deposited mica in the cave on top of unit 3. To determine the approximate age of the flood that deposited the mica in DRS1A, several charcoal samples were taken from different units from the pit that was dug. In total five pieces of charcoal

were sent to Beta Analytic for radiocarbon dating analysis. The results of this analysis are shown in **APPENDIX; Table 6**.

The next rock shelter we examined for paleofloods was DRS1B. This rock shelter is located approximately 3.7 m in elevation higher and 3 m further downstream than DRS1A. Inside DRS1B we dug small pit in the south corner of the shelter. The surface of this pit that we dug appeared to be an abandoned buzzard's nest, so the pit was named "Buzzard Pit." The elevation of the surface of DRS1B-BP was measured to be 279.68 m asl. **Figure 15** shows the stratigraphic description for the pit.

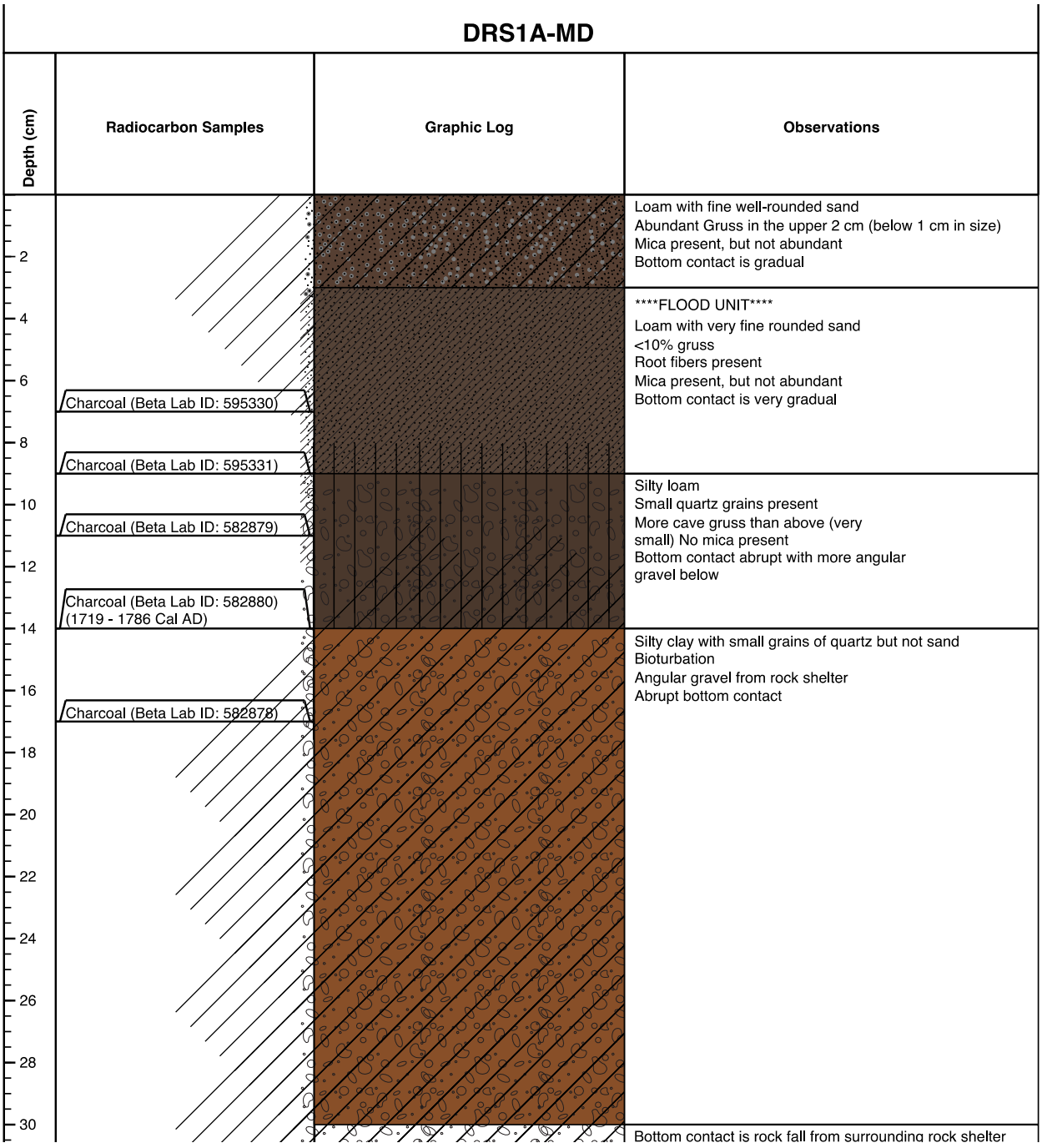

Figure 14: The stratigraphic description of DRS1A-MD, as well as the observations made and radiocarbon sample locations. This rock shelter is the lowest of three rock shelters located at the Douglas Tailwater site.

Based on the stratigraphy observed in DRS1B-BP we determined that at least one flood, potentially two, reached the height of this rock shelter. The case for two floods is as follows:

Units 3 and 4 are likely one flood event and units 1 and 2 are likely another. The reasoning behind this idea of two flood events is because of the cave gruss. Gruss is composed of small rocks that have been broken down from rock that makes up the rock shelter itself. The first flood that occurred would have deposited sediment in the cave filling in the gaps between the gruss that was observed in unit 4. The flood sediment would have also mixed with the sediment that was already present in the rock shelter. A second flood likely caused the same process to occur in the uppermost units of DRSB-BP. Due to the development of the sediment, it is unlikely that one flood event filled in the pore spaces at the same time. It is much more likely that two separate large flood events deposited mica rich sediment into the rock shelter. Unfortunately, no charcoal found in DRS1B-BP was large enough for radiocarbon dating analysis.

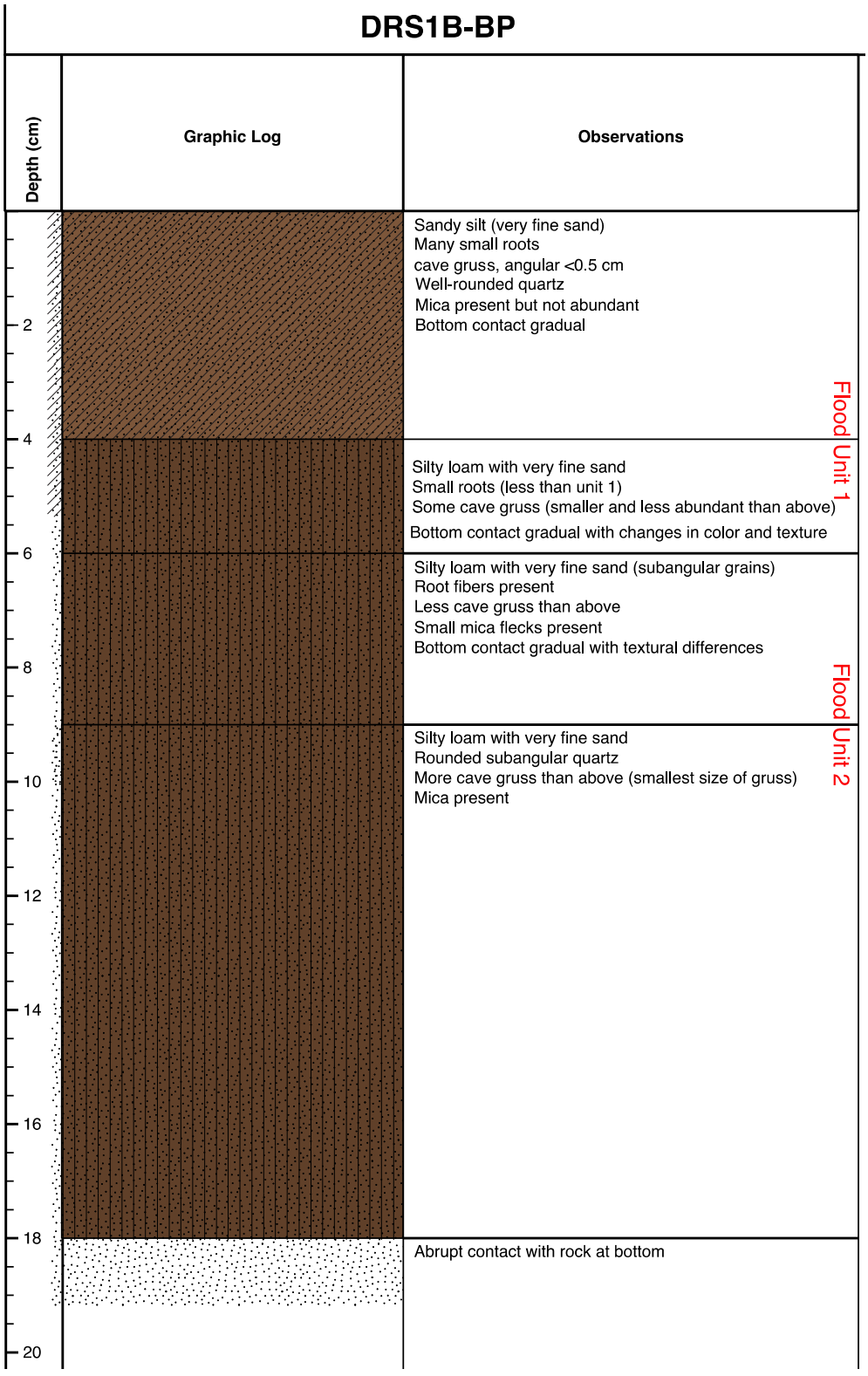

Figure 15: The stratigraphic description for DRS1B-BP including observations made about each stratigraphic unit. This rock shelter is the middle of three rock shelters located at the Douglas Tailwater site.

The third rock shelter that was identified was DRS1C. This rock shelter is located near the top of the ridge. The elevation of the mouth of DRS1C was measured to be 287.3 m asl. This puts DRS1C ~2.3 m in elevation above DRS1B. We dug very shallow pit in DRS1C, and no evidence of flood material was found. This indicates that DRS1C is the upper limit of our flood chronology.

Based on the stratigraphic descriptions of DRS1A-MD and DRS1B-BP, several floods have likely been preserved. Currently, for the French Broad River, the flood of record was in 1867. This flood had a discharge of 5,380.20 m^3/s at the DT site. This discharge was calculated using the HEC-RAS model based on the TVA Flood Profile for the 1867 flood. The TVA Flood Profile from 1940 has the water surface elevation of the 1867 flood at 273.7 m asl. This puts the stage height of the 1867 flood ~2.3 meters below the mouth of DRS1A. Since the 1867 flood did not reach any of the rock shelters at DT, older and larger flood(s) must be responsible for the deposits. Radiocarbon dates from DRS1A indicate that the age of the charcoal pieces deposited in the flood waters range in age from 1719-1942. Since there is a flood record provided by a USGS gauge 470 m downstream of DRS1 (USGS stream gauge 03469000) that dates to the 1867 flood there is a high level of confidence that there have been no unrecorded large floods since that time. A TVA report from 1961 describes several larger floods on the French Broad River. The largest of which was the April 1791 flood. This is likely the flood that deposited the charcoal along with fluvial sediment in DRS1A. The report also lists the floods of August 1796, May 1845, and August 1852 as having higher stages than the August 1928 flood.

Based on the flood history of the French Broad River and the radiocarbon dates from DRS1A, it is likely that several large floods in the late 1700s were responsible for depositing

fluvial sediments in the rock shelters at DT. Since there is evidence of flooding in DRS1B-BP, it is possible that at least one flood affected both DRS1A and DRS1B.

4.4 Combined flood chronology

By combining the two sites' flood histories, a more complete record of flooding in the Upper French Broad River was established, extending the flood record to the early-to-mid 1700s. Floods were identified at the DT3A site using positive residuals and a robust age-depth model. This information was tied to the radiocarbon samples that were found in the DRS site to provide a more complete flood history for the watershed as shown in **Figure 16**. This combined record indicates that there are at least four large flood events that occurred after 1700 that have similar or larger positive residuals to that of the 1876 flood of record. The floods of 1769, 1744, and 1732 are floods that have not been referenced in historical documentation and are unlikely to have been considered when the current flood frequency analysis was done for this area. The 1744 flood has multiple peaks associated with it because this depth is where there was a break in the core resulting in a large age range for this event. The three floods that were identified in the DRS site are all prior to the 1867 flood as well. The DRS flood events have a minimum discharge that was determined using the HEC-RAS model that was constructed. The minimum discharge for all three of the flood events that were identified based on radiocarbon samples found in DRS1-A is 8,155.25 m^3/s. Flood deposits were also identified in DRS1-B, which indicates that at least one flood with a minimum discharge of 13110.70 m^3/s occurred on the French Broad River. Since there was no datable material found in DRS1B, the exact date of the flood is unknown. While there is no datable evidence of floods in DRS1-B, the largest flood based on the positive residuals from the DT3A site are from 1796. This would indicate that the likely candidate for the largest flood that was discovered from this study was the flood from 1796, which would have

had a discharge that would have exceeded 13,110.70 m^3/s. By knowing what the minimum discharge for the three largest floods based on their positive residuals, this allows this information to be used to expand upon the flood record for this site. As stated in the USGS's Bulletin 17C, paleofloods can be included in flood frequency analyses, and are treated the same as a historical flood would be (England, et al., 2019).

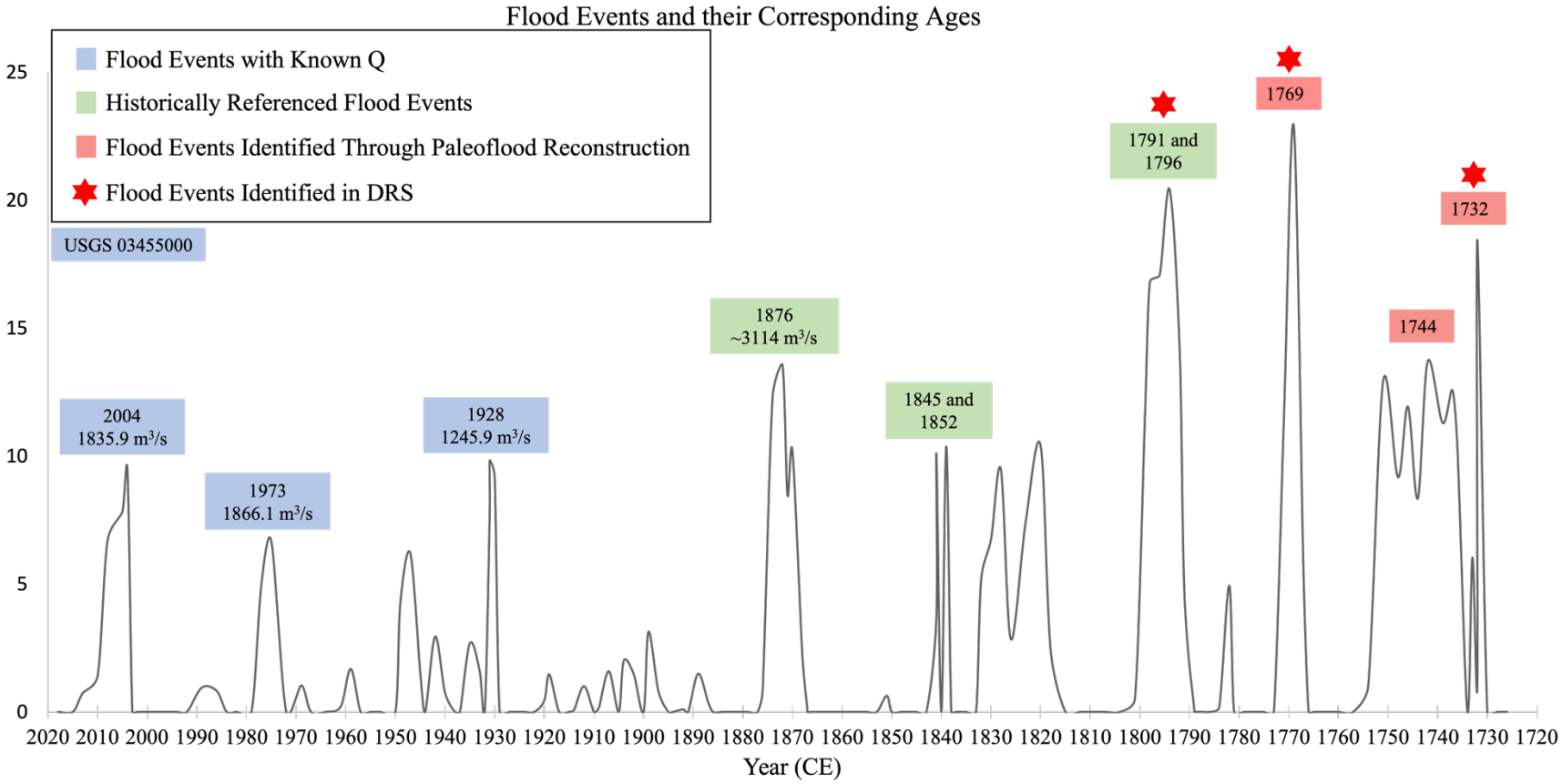

Figure 16: A paleoflood chronology constructed using, USGS stream gauge data (03455000), historically referenced flood events, positive residuals of sand, the BACON age-depth model from site DT3A, and the flood events recorded at DRS site.

5. DISCUSSION

5.1 Paleofloods on the French Broad River

This study extends the continuous flood record on the French Broad River from 100 years to a record of nearly more than three times that. This 290-year record provides a history of large floods on the French Broad River over a much longer time scale than that of any instrumented record in the southeastern United States. From this new record, we can see a trend that shows decreasing positive residuals for flood events in recent history, as compared to flood events from the 1700s and early 1800s. Since positive residuals are correlated to flood magnitude (Leigh, 2018), it indicates that flood magnitude has likely decreased over time since the 1700s.

5.2 Paleoflood trends in the region

This study identified three flood events that have positive residuals at least 1.5 times larger than the flood of record for the river. These events would suggest that flood magnitudes were higher during previous time periods. This is supported by a study upstream of this study site in the southern Blue Ridge Mountains. Wang and Leigh (2012) found that the extreme floods in their record occurred at transitional times in the Earth's climate. These transitional times, such as at the beginning and end of the MCA and LIA, were periods of extreme wetness (Wang and Leigh, 2012). The record of this study extends back to the transitional period after the LIA, which is where the largest floods identified are located. This suggests that the study site for this work is also greatly influenced by transitional climates.

On the Nolichucky River (a tributary of the French Broad River) Anderson et al. reconstructed summer streamflow conditions (2019). While this study only focuses on streamflow during a particular time of year, they identified a period of extremely high streamflow in the 1730s (Anderson et al., 2019). This lines up with the first large flood event that was identified through this study in 1732. A double peak centered around 1825 is also found in the Nolichucky River as well as in our reconstruction. Since the Anderson et al. (2019) study examines streamflow during May, June, and July it does not record the other significant flood events identified in our study. It does however provide information about the spatial extent of high flow conditions throughout the region. Additional studies could provide information that would allow better discernment of causes of particular flooding events.

Approximately 200 km downstream from the Douglas study sites, Harden et al. (2021) found evidence of one of the largest floods in U.S. history at a site near Chattanooga, Tennessee. This flood occurred sometime between 1650 and 1700 C.E. and had a discharge of over 1,000,000 ft^3/s (>28,000 m3/s) (Harden et al., 2021a). This event also corresponds well with the ending of the LIA, again supporting the idea that extreme floods are occurring during periods of climate transition. These extreme events are all occurring within the LIA, however there is no single agreed upon end date for the LIA (Rodysill et al., 2018). Since the date varies by ~100 years it is important to not focus on the period, but rather what influences the LIA was having climactically. These climatic influences can cause large and abrupt changes in both flood frequency and magnitude (Knox, 1993).

On a larger scale, Munoz and Dee (2017) identified how a larger climate forcing mechanism influences discharge and flooding on the Mississippi River. By looking at major flood events on the lower Mississippi River and correlating them to El Niño events, they found

that a warm ENSO phase, preconditions the Mississippi River to be vulnerable to flooding (Munoz and Dee, 2017). This preconditioning occurs because the increased precipitation associated with a warm ENSO phase reduces the infiltration capacity of the soil in the basin resulting in flooding (Munoz and Dee, 2017). It is has also been noted that AMO strongly influences the inland flux of moisture from the Gulf of Mexico (Tootle and Piechota, 2006; Munoz et al., 2018; Anderson et al., 2019; Sadeghi et al., 2019). The inland flux of moisture associated with AMO also results in flooding by carrying large amounts of water inland in the form of hurricanes. With the strong correlation shown between AMO and streamflow and precipitation in the southeast U.S. it is possible that some of the flood events identified in this study are caused by the AMO being in positive phase.

5.3 Sources of Error

The location of the two study sites is likely to cause some disconnect in the magnitude and frequency of flood events recorded. Since DT3A is located upstream from where the Pigeon and Nolichucky Rivers join the French Broad River, there is less water flowing through this site as compared to DRS. While the discrepancy in discharge may be more noticeable during more moderate flow events, during extreme flood events sediments would likely still be deposited at both sites. An example of this can be seen in the streamflow reconstruction of the Nolichucky River. One of the largest discharges was identified in the early 1730s and evidence of this flood was also found at the DT3A site (Anderson et al., 2019). This is due to the nature of the events that are causing extreme flood events, such as hurricanes, rain on snow events, and large convective systems moving through the region (Tennessee Valley Authority, 1940). These events are unlikely to impact just one of the tributaries of the French Broad River without affecting the French Broad River itself.

The record developed in this study does not include every extreme flood event that has occurred on the French Broad River over the time scale that was captured. One reason that floods are missing from this record is because of the unique nature of flood events and the physics of how they deposit or erode sediment. Large flood events do not always deposit sediments onto a floodplain, and in some cases they can erode sediments deposited by previous flood events (Leigh, 2018; Toonen et al., 2020). Also, this study's methodology differs from that of previous works in that the entire sand population was used for the reconstruction. In previous works (Toonen et al., 2015, 2020; Leigh, 2018) just the coarsest fraction of the particle size data was used to identify flood events. While the method used in this study was able to identify several flood events, the use of a larger range of particle sizes could decrease the detection limit of extreme floods. Including the smaller fraction of the sand population in the analysis allows for the potential misinterpretation of peaks. This misinterpretation of peaks is due to the fact that smaller sediment has a greater probability of being transported and deposited from a source other than the French Broad River (i.e., hillslope runoff). This can also result in false flood peaks. As evident from the lack of flood event during 1948, which was identified as a flood based on positive residuals but is not supported by the instrumented peak flow record. Additionally, some floods from the instrumental record were not identified in the positive residuals. For example, the flood of 1965 has a larger discharge than some of the reconstructed floods identified, but no positive residual peak from the LOESS analysis corresponds with this flood. This can be explained by understanding the way the LOESS function works. The function creates a smooth trendline through a data set based on multiple overlapping regressions applied to subsets of the data to produce a general trend that incorporates localized variability. Therefore, if a section of the sediment core was sandy, the trendline would increase. This could cause a peak of extreme

sand to be minimized because the function is overall trending upward. Since the entire sand fraction was included instead of just the coarsest end member, many floods likely did not generate positive residuals large enough to be above the trendline, which was interpreted as a threshold identified large and extreme floods. Despite these limitations, there is some confidence to be had in the identification of the three largest flood events (all in the 1700s). The 1791 flood was written about in historical accounts, providing validation for this event. The ages of these three floods also overlapped with the ages of floods found in the DRS1 (rock shelter) site downstream where the flood magnitude is much better constrained. This suggests that these high magnitude floods carried much larger volumes of sand than other floods in the reconstructed record, allowing their positive residuals to peak well above the LOESS trendline. Furthermore, this also suggests that volumetric sand measurements may be a better proxy for identifying large and extreme floods over particle descriptors, such as the D90. Future studies should aim to make direct comparisons of both approaches to discern differences in the resulting reconstructed records.

While this new record of extreme floods on the French Broad River may not capture all extreme events during this period, the flood events that were identified are still able to provide valuable information. The information gained can help to better understand the frequency and the possible drivers of the extreme flood events. To help remedy this in future work, more study sites should be selected and analyzed along the river to better identify all flood events.

Additionally, identifying the relationship between magnitude and particle size would help provide a more robust paleoflood record. This study has helped highlight the frequency of extreme flood events, but by identifying the relationship between particle size and discharge of extreme flood events, a more robust flood chronology could be built (Toonen et al., 2015; Leigh,

2018). In this study, discharges of some of the largest floods were determined by applying the discharges of commonly occurring floods reconstructed at DRS site.

The resolution of the particle size analysis can also add uncertainty into the final analysis. Sampling at a 1 cm resolution for particle size, censors information about both smaller flood events, as well as large flood events that deposited less than 1 cm of sediment. Sampling at a finer resolution, however, poses other challenges. The main challenge is having enough sample for particle size analysis and dating techniques to be done.

6. CONCLUSIONS

This research set out to identify, date, and quantify extreme flood events that occurred prior to the installation of stream gauges on the French Broad River in northeastern Tennessee. By studying the sediments deposited by flood events on floodplains and in rock shelters, the flood record for the French Broad River was extended from just over 100 years to a record of almost 300 years. This new record adds three flood events that likely exceeded the current flood of record's magnitude by at a minimum, one and a half times. Additionally, the trends that were observed at this study site were seen at sites across the southeastern United States. This indicates that climate transitions are periods that experience significant extreme flood events. However, to better understand the relationship between sediment size and discharge of the river, more work is needed.

This discovery highlights the need for more quantitative paleoflood studies. As floods become more impactful to human life across the world, we need to have a better understanding of the risk associated with them. By lengthening our streamflow records, we can better prepare for floods in the future by including these paleofloods in flood frequency models. Applying these techniques to other watersheds would allow us to better understand the impact that humans are having on flood events and help preserve human life and property.

REFERENCES

Abbasi, A., 2019, 210Pb and 137Cs based techniques for the estimation of sediment chronologies and sediment rates in the Anzali Lagoon, Caspian Sea: Journal of Radioanalytical and Nuclear Chemistry, v. 322, p. 319–330, doi:10.1007/S10967-019-06739-8.

Alipour, A., Ahmadalipour, A., and Moradkhani, H., 2020, Assessing flash flood hazard and damages in the southeast United States: Journal of Flood Risk Management, v. 13, p. e12605, doi:https://doi.org/10.1111/jfr3.12605.

Anderson, S., Ogle, R., Tootle, G., and Oubeidillah, A., 2019, Tree-Ring Reconstructions of Streamflow for the Tennessee Valley: Hydrology , v. 6, doi:10.3390/hydrology6020034.

Anselmetti, F.S., Schulte, L., and Stoffel, M., 2020, Paleofloods: changes in prehistoric flood occurrence: ETH Zurich.

Arcement, G.J., and Schneider, V.R., 1989, Guide for selecting Manning's roughness co-efficients for natural channels and flood plains. : U.S. Geological Survey water-supply paper ; : U.S. Geological Survey water-supply paper ; Department of the Interior, U.S. Geological Survey, U.S. Geological Survey water-supply paper: 2339, http://libdata.lib.ua.edu/login?url=https://search.ebscohost.com/login.aspx?direct=true&db=cat00456a&AN=ua.1370265&site=eds-live&scope=site.

Baker, V.R., 2008, Paleoflood hydrology: Origin, progress, prospects: Geomorphology, v. 101, p. 1–13, doi:https://doi.org/10.1016/j.geomorph.2008.05.016.

Ballesteros-Cánovas, J.A., Stoffel, M., St George, S., and Hirschboeck, K., 2015, A review of flood records from tree rings: Progress in Physical Geography: Earth and Environment, v. 39, p. 794–816, doi:10.1177/0309133315608758.

Benito, G., Harden, T.M., and O'Connor, J., 2022, 6.35 - Quantitative Paleoflood Hydrology, *in* Shroder, J. (Jack) F.B.T.-T. on G. (Second E. ed., Oxford, Academic Press, p. 743–764, doi:https://doi.org/10.1016/B978-0-12-409548-9.12495-9.

Benito, G., and O'Connor, J.E., 2013, 9.24 Quantitative Paleoflood Hydrology, *in* Shroder, J.F.B.T.-T. on G. ed., San Diego, Academic Press, p. 459–474, doi:https://doi.org/10.1016/B978-0-12-374739-6.00250-5.

Berghuijs, W.R., Aalbers, E.E., Larsen, J.R., Trancoso, R., and Woods, R.A., 2017, Recent changes in extreme floods across multiple continents: Environmental Research Letters, v. 12, p. 114035, doi:10.1088/1748-9326/aa8847.

Beyraghdar Kashkooli, O., and Modarres, R., 2020, Is the volatility and non-stationarity of the Atlantic Multidecadal Oscillation (AMO) changing? Global and Planetary Change, v. 189, p. 103160, doi:https://doi.org/10.1016/j.gloplacha.2020.103160.

Blaauw, M., and Christen, J.A., 2011, Flexible paleoclimate age-depth models using an autoregressive gamma process: Bayesian Analysis, v. 6, p. 457–474, doi:10.1214/11-BA618.

Blum, A.G., Ferraro, P.J., Archfield, S.A., and Ryberg, K.R., 2020, Causal Effect of Impervious Cover on Annual Flood Magnitude for the United States: Geophysical Research Letters, v. 47, p. e2019GL086480, doi:https://doi.org/10.1029/2019GL086480.

Bregy, J.C., Wallace, D.J., Minzoni, R.T., and Cruz, V.J., 2018, 2500-year paleotempestological record of intense storms for the northern Gulf of Mexico, United States: Marine Geology, v. 396, p. 26–42, doi:10.1016/J.MARGEO.2017.09.009.

Chang, H., Franczyk, J., and Kim, C., 2008, What is responsible for increasing flood risks? The case of Gangwon Province, Korea: Natural Hazards, v. 48, p. 339, doi:10.1007/s11069-008-9266-y.

Curtis, S., 2008, The Atlantic multidecadal oscillation and extreme daily precipitation over the US and Mexico during the hurricane season: Climate Dynamics, v. 30, p. 343–351, doi:10.1007/s00382-007-0295-0.

Denniston, R.F., and Luetscher, M., 2017, Speleothems as high-resolution paleoflood archives: Quaternary Science Reviews, v. 170, p. 1–13, doi:https://doi.org/10.1016/j.quascirev.2017.05.006.

Ely, L.L., and Baker, V.R., 1985, RECONSTRUCTING PALEOFLOOD HYDROLOGY WITH SLACKWATER DEPOSITS: VERDE RIVER, ARIZONA: Physical Geography, v. 6, p. 103–126, doi:10.1080/02723646.1985.10642266.

England, John F., J., Cohn, T.A., Faber, B.A., Stedinger, J.R., Thomas, Wilbert O., J., Veilleux, A.G., Kiang, J.E., and Mason, Robert R., J., 2019, Guidelines for Determining Flood Flow Frequency Bulletin 17C Book 4, Hydrologic Analysis and Interpretation: 148 p., https://pubs.usgs.gov/tm/04/b05/tm4b5.pdf.

Fang, K., Chen, D., Ilvonen, L., Pasanen, L., Holmström, L., Seppä, H., Huang, G., Ou, T., and Linderholm, H., 2019, Oceanic and atmospheric modes in the Pacific and Atlantic Oceans since the Little Ice Age (LIA): Towards a synthesis: Quaternary Science Reviews, v. 215, p. 293–307, doi:https://doi.org/10.1016/j.quascirev.2019.05.014.

Graves, B.P., Ralph, T.J., Hesse, P.P., Westaway, K.E., Kobayashi, T., Gadd, P.S., and Mazumder, D., 2019, Macro-charcoal accumulation in floodplain wetlands: Problems and prospects for reconstruction of fire regimes and environmental conditions: PLOS ONE, v. 14, p. e0224011, https://doi.org/10.1371/journal.pone.0224011.

Hardeman, W.D., Miller, R.A., and Swingle, G.D., 1966, Geologic map of Tennessee: Tennessee Division of Geology, v. State Geol.

Harden, T.M., and O'Connor, J.E., 2017, Prehistoric floods on the Tennessee River—Assessing the use of stratigraphic records of past floods for improved flood-frequency analysis:, doi:10.3133/sir20175052.

Harden, T.M., O'Connor, J.E., Carr, M.L., and Keith, M., 2021a, Improving flood-frequency analysis with a 4,000-year record of flooding on the Tennessee River near Chattanooga, Tennessee:, doi:10.3133/sir20205138.

Harden, T.M., Ryberg, K.R., O'Connor, J.E., Friedman, J.M., and Kiang, J.E., 2021b, Historical and paleoflood analyses for probabilistic flood-hazard assessments—Approaches and review guidelines:, doi:10.3133/tm4B6.

Hemmati, M., Ellingwood, B.R., and Mahmoud, H.N., 2020, The Role of Urban Growth in Resilience of Communities Under Flood Risk: Earth's Future, v. 8, p. e2019EF001382, doi:https://doi.org/10.1029/2019EF001382.

Hosking, J.R.M., and Wallis, J.R., 1986, Paleoflood Hydrology and Flood Frequency Analysis: Water Resources Research, v. 22, p. 543–550, doi:https://doi.org/10.1029/WR022i004p00543.

Huang, P.M., and Wang, M.K., 2005, MINERALS, PRIMARY, *in* Hillel, D.B.T.-E. of S. in the E. ed., Oxford, Elsevier, p. 500–510, doi:https://doi.org/10.1016/B0-12-348530-4/00464-1.

IPCC, 2022, Climate Change 2022: Impacts, Adaptations and Vulnerabilitiy: Cambridge University Press.

Jarrett, R.D., and England Jr., J.F., 2002, Reliability of Paleostage Indicators for Paleoflood Studies: Ancient Floods, Modern Hazards, p. 91–109, doi:https://doi.org/10.1029/WS005p0091.

Johanna, M., Giuliano, D.B., and Maurizio, M., 2022, Nighttime light data reveal how flood protection shapes human proximity to rivers: Science Advances, v. 4, p. eaar5779, doi:10.1126/sciadv.aar5779.

Jonkman, S.N., 2005, Global perspectives on loss of human life caused by floods: Natural Hazards, v. 34, p. 151–175, doi:10.1007/s11069-004-8891-3.

Kim, S., Zhang, R., Pham, H., and Sharma, A., 2019, A Review of Satellite-Derived Soil Moisture and Its Usage for Flood Estimation: Remote Sensing in Earth Systems Sciences, v. 2, p. 225–246, doi:10.1007/s41976-019-00025-7.

Knox, J.C., 2006, Floodplain sedimentation in the Upper Mississippi Valley: Natural versus human accelerated: Geomorphology, v. 79, p. 286–310, doi:https://doi.org/10.1016/j.geomorph.2006.06.031.

Knox, J.C., 1993, Large increases in flood magnitude in response to modest changes in climate: Nature, v. 361, p. 430–432, doi:10.1038/361430a0.

Lam, D., Thompson, C., Croke, J., Sharma, A., and Macklin, M., 2017, Reducing uncertainty with flood frequency analysis: The contribution of paleoflood and historical flood information: Water Resources Research, v. 53, p. 2312–2327, doi:https://doi.org/10.1002/2016WR019959.

Leigh, D.S., 2018, Vertical accretion sand proxies of gaged floods along the upper Little Tennessee River, Blue Ridge Mountains, USA: Sedimentary Geology, v. 364, p. 342–350, doi:https://doi.org/10.1016/j.sedgeo.2017.09.007.

Lemiszki, P.J., and Price, R.C., 2005, Geologic Map and Mineral Resources Summary of the Newport Quadrangle.:

Levish, D.R., 2002, Paleohydrologic Bounds: Ancient Floods, Modern Hazards, p. 175–190, doi:https://doi.org/10.1029/WS005p0175.

Li-An, C., Billa, L., and Azari, M., 2018, Anthropocene climate and landscape change that increases flood disasters: International Journal of Hydrology, v. 2, p. 487–491, doi:10.15406/ijh.2018.02.00115.

Li, S., Zhang, J.M., Xu, W.L., Wang, Y.R., Peng, Y., Li, J.N., He, X.L., and Li, P., 2014, Sensitivity Analysis of Parameters in HEC-RAS Software: Applied Mechanics and Materials, v. 641–642, p. 201–204, doi:10.4028/www.scientific.net/AMM.641-642.201.

Liu, T., Greenbaum, N., Baker, V.R., Ji, L., Onken, J., Weisheit, J., Porat, N., and Rittenour, T., 2020, Paleoflood hydrology on the lower Green River, upper Colorado River Basin, USA: An example of a naturalist approach to flood-risk analysis: Journal of Hydrology, v. 580, p. 124337, doi:https://doi.org/10.1016/j.jhydrol.2019.124337.

Lombardi, R., Davis, L., and Therrell, M.D., 2021, Flood variability in the common era: a synthesis of sedimentary records from Europe and North America: Physical Geography, p. 1–15, doi:10.1080/02723646.2021.1890894.

Maharjan, L., and Shakya, N.M., 2016, Comparative Study of One Dimensional and Two Dimensional Steady Surface Flow Analysis: Journal of Advanced College of Engineering and Management, v. 2, p. 15, doi:10.3126/jacem.v2i0.16095.

Mann, M.E., Zhang, Z., Rutherford, S., Bradley, R.S., Hughes, M.K., Shindell, D., Ammann, C., Faluvegi, G., and Ni, F., 2009, Global Signatures and Dynamical Origins of the Little Ice Age and Medieval Climate Anomaly: Science, v. 326, p. 1256–1260, doi:10.1126/science.1177303.

Margold, M., Jansen, J.D., Codilean, A.T., Preusser, F., Gurinov, A.L., Fujioka, T., and Fink, D., 2018, Repeated megafloods from glacial Lake Vitim, Siberia, to the Arctic Ocean over the past 60,000 years: Quaternary Science Reviews, v. 187, p. 41–61, doi:https://doi.org/10.1016/j.quascirev.2018.03.005.

McLauchlan, K., 2003, Plant cultivation and forest clearance by prehistoric North Americans: pollen evidence from Fort Ancient, Ohio, USA: The Holocene, v. 13, p. 557–566, doi:10.1191/0959683603hl646rp.

Miller, R.M., 1969, The Failure of the Colony of Georgia Under the Trustees: The Georgia Historical Quarterly, v. 53, p. 1–17, http://www.jstor.org/stable/40578924.

Milly, P.C.D., Wetherald, R.T., Dunne, K.A., and Delworth, T.L., 2002, Increasing risk of great floods in a changing climate: Nature, v. 415, p. 514–517, doi:10.1038/415514a.

Munoz, S.E., and Dee, S.G., 2017, El Niño increases the risk of lower Mississippi River flooding: Scientific Reports, v. 7, p. 1772, doi:10.1038/s41598-017-01919-6.

Munoz, S.E., Giosan, L., Therrell, M.D., Remo, J.W.F., Shen, Z., Sullivan, R.M., Wiman, C., O'Donnell, M., and Donnelly, J.P., 2018, Climatic control of Mississippi River flood hazard amplified by river engineering: Nature, v. 556, p. 95–98, doi:10.1038/nature26145.

Muñoz, S.E., Porter, T.J., Bakkelund, A., Nusbaumer, J., Dee, S.G., Hamilton, B., Giosan, L., and Tierney, J.E., 2020, Lipid Biomarker Record Documents Hydroclimatic Variability of the Mississippi River Basin During the Common Era: Geophysical Research Letters, v. 47, p. e2020GL087237, doi:10.1029/2020GL087237.

National Oceanic and Atmospheric Administration, 2020, 2020 National Hydrologic Assessment:, https://www.nws.noaa.gov/oh/2020_National_Hydrologic_Assessment.pdf.

NRCS, U. Web Soil Survey:, https://websoilsurvey.sc.egov.usda.gov/App/HomePage.htm (accessed September 2021).

O'Connor, J.E., and Webb, R.H., 1988, Hydraulic modeling for paleoflood analysis: Flood Geomorphology. John Wiley & Sons New York. 1988. p 393-402. 7 fig, 1 tab, 24 ref.,.

O'Geen, A., 2007, Soils: Genesis and Geomorphology: New York, Cambridge University Press, v. 6, 265–265 p., doi:10.2136/vzj2007.0030br.

Onda, Y., Gomi, T., Mizugaki, S., Nonoda, T., and Sidle, R.C., 2010, An overview of the field and modelling studies on the effects of forest devastation on flooding and environmental issues: Hydrological Processes, v. 24, p. 527–534, doi:https://doi.org/10.1002/hyp.7548.

Owens, M.J., Lockwood, M., Hawkins, E., Usoskin, I., Jones, G.S., Barnard, L., Schurer, A., and Fasullo, J., 2017, The Maunder minimum and the Little Ice Age: an update from recent reconstructions and climate simulations: J. Space Weather Space Clim., v. 7, https://doi.org/10.1051/swsc/2017034.

Pielke, R.A., and Downton, M.W., 2000, Precipitation and Damaging Floods: Trends in the United States, 1932–97: Journal of Climate, v. 13, p. 3625–3637, doi:10.1175/1520-0442(2000)013<3625:PADFTI>2.0.CO;2.

Rapuc, W. et al., 2019, Holocene-long record of flood frequency in the Southern Alps (Lake Iseo, Italy) under human and climate forcing: Global and Planetary Change, v. 175, p. 160–172, doi:https://doi.org/10.1016/j.gloplacha.2019.02.010.

Reinders, J.B., and Muñoz, S.E., 2021, Improvements to Flood Frequency Analysis on Alluvial Rivers Using Paleoflood Data: Water Resources Research, v. 57, p. e2020WR028631, doi:https://doi.org/10.1029/2020WR028631.

Rodysill, J.R. et al., 2018, A North American Hydroclimate Synthesis (NAHS) of the Common Era: Global and Planetary Change, v. 162, p. 175–198, doi:https://doi.org/10.1016/j.gloplacha.2017.12.025.

Sadeghi, S., Tootle, G., Elliott, E., Lakshmi, V., Therrell, M., Kam, J., and Bearden, B., 2019, Atlantic Ocean Sea Surface Temperatures and Southeast United States streamflow variability: Associations with the recent multi-decadal decline: Journal of Hydrology, v. 576, p. 422–429, doi:https://doi.org/10.1016/j.jhydrol.2019.06.051.

Schillereff, D.N., Chiverrell, R.C., Macdonald, N., and Hooke, J.M., 2014, Flood stratigraphies in lake sediments: A review: Earth-Science Reviews, v. 135, p. 17–37, doi:https://doi.org/10.1016/j.earscirev.2014.03.011.

Springer, G.S., and Kite, J.S., 1997, River-derived slackwater sediments in caves along Cheat River, West Virginia: Geomorphology, v. 18, p. 91–100, doi:https://doi.org/10.1016/S0169-555X(96)00022-0.

Stoffel, M., and Corona, C., 2014, Dendroecological Dating of Geomorphic Disturbance in Trees: Tree-Ring Research, v. 70, p. 3–20, doi:10.3959/1536-1098-70.1.3.

Strupczewski, W.G., Kochanek, K., and Bogdanowicz, E., 2014, Flood frequency analysis supported by the largest historical flood: Nat. Hazards Earth Syst. Sci., v. 14, p. 1543–1551, doi:10.5194/nhess-14-1543-2014.

Tennessee Valley Authority, (TVA), 2020, Douglas:, https://www.tva.com/energy/our-power-system/hydroelectric/douglas (accessed February 2022).

Tennessee Valley Authority, (TVA), 1940, Flood History of French Broad River and its Tributaries: v. 1.

Tennessee Valley Authority, (TVA), 1961, Floods and Flood Control: Tennessee Valley Authority, Technical report, 26, 302 p., https://books.google.com/books?id=9FvVAAAAMAAJ.

Thabane, L. et al., 2013, A tutorial on sensitivity analyses in clinical trials: the what, why, when and how: BMC Medical Research Methodology, v. 13, p. 92, doi:10.1186/1471-2288-13-92.

Toonen, W.H.J., Munoz, S.E., Cohen, K.M., and Macklin, M.G., 2020, High-Resolution Sedimentary Paleoflood Records in Alluvial River Environments: A Review of Recent Methodological Advances and Application to Flood Hazard Assessment BT - Palaeohydrology: Traces, Tracks and Trails of Extreme Events, *in* Herget, J. and Fontana, A. eds., Cham, Springer International Publishing, p. 213–228, doi:10.1007/978-3-030-23315-0_11.

Toonen, W.H.J., Winkels, T.G., Cohen, K.M., Prins, M.A., and Middelkoop, H., 2015, Lower Rhine historical flood magnitudes of the last 450years reproduced from grain-size measurements of flood deposits using End Member Modelling: CATENA, v. 130, p. 69–81, doi:https://doi.org/10.1016/j.catena.2014.12.004.

Tootle, G.A., and Piechota, T.C., 2006, Relationships between Pacific and Atlantic ocean sea surface temperatures and U.S. streamflow variability: Water Resources Research, v. 42, doi:https://doi.org/10.1029/2005WR004184.

United States Geologic Survey, 2020, Gages Through the Ages:, https://labs.waterdata.usgs.gov/visualizations/gages-through-the-ages/index.html#/ (accessed May 2022).

USACE, U.S.A.C. of E., 2022, Hydrologic Engineering Center River Analysis System (HEC-RAS):, https://www.hec.usace.army.mil/software/hec-ras/.

Victoriano, A., Díez-Herrero, A., Génova, M., Guinau, M., Furdada, G., Khazaradze, G., and Calvet, J., 2018, Four-topic correlation between flood dendrogeomorphological evidence and hydraulic parameters (the Portainé stream, Iberian Peninsula): CATENA, v. 162, p. 216–229, doi:https://doi.org/10.1016/j.catena.2017.11.009.

Wang, L., and Leigh, D.S., 2012, Late-Holocene paleofloods in the Upper Little Tennessee River valley, Southern Blue Ridge Mountains, USA: The Holocene, v. 22, p. 1061–1066, doi:10.1177/0959683612437863.

WATERS, and Environmental Protection Agency, 2020, Watershed Assessment, Tracking & Environmental Results System (WATERS):, https://www.epa.gov/waterdata/viewing-waters-data-using-google-earth.

Webb, R.H., and Jarrett, R.D., 2002, One-Dimensional Estimation Techniques for Discharges of Paleofloods and Historical Floods: Ancient Floods, Modern Hazards, p. 111–125, doi:https://doi.org/10.1029/WS005p0111.

Yang, A., Wang, H., Liu, W., Hu, K., Liu, D., Wu, C., and Hu, X., 2022, Two megafloods in the middle reach of Yarlung Tsangpo River since Last-glacial period: Evidence from giant bars: Global and Planetary Change, v. 208, p. 103726, doi:https://doi.org/10.1016/j.gloplacha.2021.103726.

Yin, H., and Li, C., 2001, Human impact on floods and flood disasters on the Yangtze River: Geomorphology, v. 41, p. 105–109, doi:https://doi.org/10.1016/S0169-555X(01)00108-8.

Zielhofer, C., Recio Espejo, J.M., Núnez Granados, M.À., and Faust, D., 2009, Durations of soil formation and soil development indices in a Holocene Mediterranean floodplain: Quaternary International, v. 209, p. 44–65, doi:https://doi.org/10.1016/j.quaint.2009.02.023.

APPENDIX

Table 4: The radiocarbon dating analysis for the samples pulled from DRS1A-MD

Beta Lab ID	Depth Below Surface (cm)	Date Ranges (cal AD)	Percent Confidence
595330	7	1799-1940	67.2%
		1680-1740	25.8%
		1752-1764	2.4%
595331	9	1802-1936	69.3%
		1683-1735	26.1%
582879	11	1798-1942	64.0%
		1674-1744	26.8%
		1750-1765	4.1%
		1744-1776	0.5%
582880	14	1719-1786	31.6%
		1906-Post AD 1950	19.4%
		1832-1892	17.9%
		1664-1708	16.7%
		1792-1819	9.8%
582878	17	1810-1919	68.7%
		1692-1727	26.7%